1 APRIL 1976

SPACE TELESCOPE OPTICAL TELESCOPE ASSEMBLY/SCIENTIFIC INSTRUMENTS PHASE B PRELIMINARY DESIGN AND PROGRAM DEFINITION STUDY

VOLUME IIA(3) — ASTROMETRY FINAL REPORT

Prepared for
GEORGE C MARSHALL SPACE FLIGHT CENTER
NATIONAL AERONAUTICS AND SPACE ADMINISTRATION
MARSHALL SPACE FLIGHT CENTER, ALABAMA

Under contract NAS8-29949

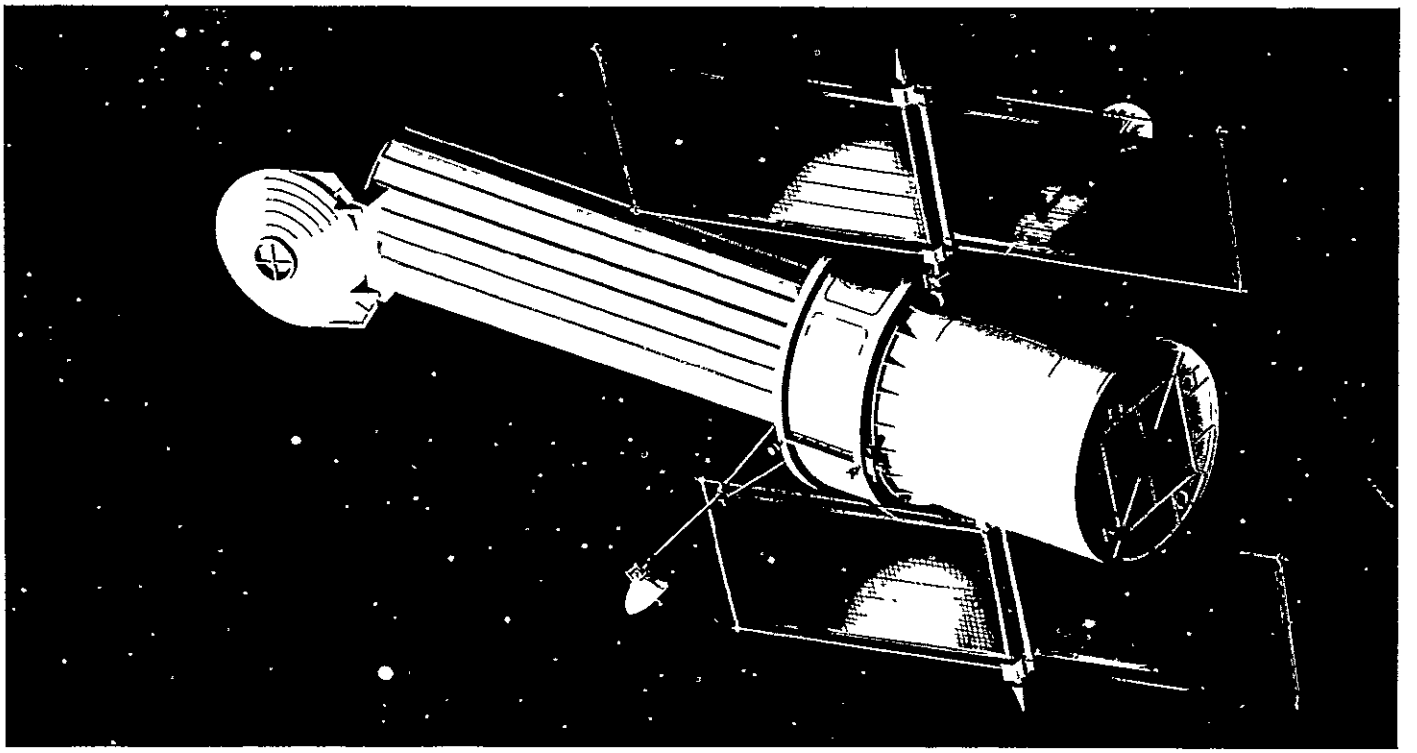

Itek
Optical Systems
A Division of Itek Corporation
10 Maguire Road
Lexington, Massachusetts 02173

Bendix
Aerospace Systems Division

MARTIN MARIETTA
DENVER DIVISION

Lockheed
MISSILES & SPACE COMPANY, INC.

VOLUME IIA (3)

ASTROMETRY FINAL REPORT

TABLE OF CONTENTS

LIST OF FIGURES

LIST OF TABLES

1.0 INTRODUCTION

Table 1.0-1 gives the astrometer instrument characterization as set forth in the SI Requirements Document, LST Scientific Instruments Requirements for Preliminary Design, revised 15 April 1975, Goddard Space Flight Center. In Itek's concept, a majority of the astrometric goals can be obtained without a specific dedicated instrument by simply utilizing a modified fine guidance sensor. Of course, additional useful data may also be gathered by other instruments (e.g., f/24 camera, faint object camera).

Wide field measurements, namely, measurements of relative angular separations between stars over a relatively wide field for parallax and proper motion determinations, are made with the third fine guidance sensor. Narrow field measurements, i.e., double star measurements, are accomplished primarily with the area photometer or faint object camera at f/96.

The wavelength range required can be met by the fine guidance sensor which has a spectral coverage from 3000 to 7500 A. The field of view of the fine guidance sensor also exceeds that required for the wide field astrometric instrument.

The requirements document requires a filter wheel for the wide-field astrometer, and so one has been incorporated into the design of the fine guidance sensor. The filter wheel probably would contain two neutral density filters to extend the dynamic range of the sensor and three spectral filters for narrowing effective double star magnitude difference. The only other changes to the fine guidance sensor to enable it to perform astrometry involve the operating modes and the command/data structure. All three fine guidance sensors are capable of astrometry.

This report is primarily concerned with the use of the fine guidance sensor (FGS) for astrometry. First, the operating principle of the FGS is described (Section 2). Then the FGS design and operation is described (Section 3) in detail relevant to its use as an astrometer. Next, (Section 4) astrometry with the FGS is described, and the complementary use of the scientific instruments and the FGS is described (Section 5).

Many more details of the FGS design and operation, including block diagrams and layout drawings, will be found in Volume IIB, Optical Telescope Assembly.

TABLE 1.0-1

ASTROMETER INSTRUMENT CHARACTERIZATION

TYPE:

A) WIDE FIELD - FINE GUIDANCE SENSOR

B) NARROW FIELD - HIGH ANGULAR/TIME RESOLUTION USING FINE GUIDANCE SENSOR, HSAP OR HRC

DETECTORS:

A) WIDE FIELD - FINE GUIDANCE SENSOR WITH IMAGE DISSECTOR

B) NARROW FIELD - FINE GUIDANCE SENSOR WITH IMAGE DISSECTOR,
HSAP WITH ICCD
HRC WITH CCD

ACQUISITION: SPACECRAFT

CALIBRATION: FINE GUIDANCE SENSOR GRATING

WAVELENGTH: RANGE 3000 - 7500 Å (4000 -6000Å REQUIRED)

F.O.V.: FINE GUIDANCE SENSOR - 3 X 15 ARCMIN. (20 SQ ARCMIN REQUIRED)
HRC - 3 X 3 ARCMIN
HSAP - 2.7 X 4 ARCSEC

UNCERTAINTY OF ANGULAR MEASUREMENTS:
FINE GUIDANCE SENSOR $\pm$ 0.002 ARCSEC

EXPOSURE TIME: ACCURACY 2% DURATION UP TO 10 MINUTES

FILTERS: 6 POSITION FILTER WHEEL IN FINE GUIDANCE SENSOR

1.0 TRADE STUDIES

Trade studies were conducted to ensure the overall feasibility of the Focal Plane Camera in a radial module. The primary variable in the trade studies was the location of the pick-off mirror; on axis versus off-axis. In addition, the impact of two alternate SECO submodules was assessed. The two alternatives were: the standard (electro-magnetic focus) SECO submodule as defined later in this report (see Section 2.4, p. 2-29 ff); and the MOD 15 permanent magnet focus SECO submodule as defined in the Princeton University Final Report, 28 February 1975, Contract NAS5-20507.

With the existing state of technology, the performance of the Focal Plane Camera is limited by the SECO submodule. Therefore, the technical areas of concern for the trade studies were primarily the packaging affected parameters of thermal dissipation, focal plane obscuration, and image quality.

Table 1.0-1 summarizes the configurations traded and the technical areas evaluated.

1.1 Radial Module Configurations

Conceptual drawings of four configurations were created to assess space availability, orbital maintainability, and focal plane obscuration.

Figure 1.1-1 is a concept drawing of a radial module utilizing an on-axis pick-off and a standard SECO submodule. The concept indicates adequate space for the filter assembly, calibration assembly, and capping shutter (provided the pick-off mirror is outside of the module envelope shown). This concept allows for orbital maintainability since the module can be removed by first guiding the module radially away from the ST axis and then rotating the module into space adjacent to the axial modules. If the axial pick-off mirror is attached to the module, then either a minimum SSM wall radius of 84 inches or an opening in the SSM wall adjacent to the radial module is required.

Figure 1.1-2 is a similar configuration to Figure 1.1-1, but utilizing the PM SECO. The larger size of this SECO submodule does not allow adequate space for the filter and calibration assemblies. This configuration is considered unsuitable for the ST.

Figure 1.1-3 shows a configuration requiring a redesign of the ST structure in the focal plane area to allow for the packaging of the PM SECO in a larger radial module. The redesign consists of designing the focal plane structure as an integral part of the primary support structure. This configuration is considered feasible; however, it effects a significant design impact and thus, a cost impact of the ST.

Figure 1.1-4 is a concept which utilizes an off-axis edge-of-field pick-off and a standard SECO submodule. In this concept, there is insufficient space to package four eight-position filter wheels. The concept drawing shows a filter assembly outline consistent with six six-position filter wheels.

TABLE 1.0-1

TRADE STUDIES

RADIAL MODULE CONFIGURATIONS

- On-Axis Pick-Off Mirror
- Off-Axis Pick-Off Mirror
- Standard SECO
- Permanent-Magnet Focus SECO

TECHNICAL AREAS EVALUATED

- Thermal Dissipation
- Focal Plane Obscuration
- Image Quality

2.0 REVIEW OF FINE GUIDANCE SENSOR AND ITS USE IN ASTROMETRY

The guide fields allotted to the three fine guidance sensors are shown in Figure 2.0-1. Each field has a maximum radius of 260 millimeters, a minimum radius of 210 millimeters, and extends 60 degrees around the periphery of the focal plane. The total guide field area is 36,913 millimeter^2 which, in object space, corresponds to an area of 11.13 mrad^2. Each sensor has an area of 3.71 mrad^2, equivalent to an area 6.6 x 6.6 arcminutes.

Figure 2.0-2, drawn from star density data in Allen, Astrophysical Quantities, shows the numbers of star available within the field of one fine guidance sensor as a function of visual magnitude. On the average, fifty stars of visual magnitude 17 or brighter would be available.

The basic concept of the fine guidance sensor is to use a fixed grating at the focal plane upon which the guide star is imaged. This grating breaks the beam from the guide star into different optical channels, and the precise location of the guide star image on the grating determines the relative balance of power in the different channels. The only element in the sensor whose stability is critical for stabilization of the telescope line-of-sight is the grating itself.

Figure 2.0-3 shows a two-dimensional version of the concept. The grating consists of prismatic grooves on the grating substrate. In the fine stabilization mode of operation, the guide star image lies at the bottom (or at the ridge) of one of the grooves. The portion of the image falling on one facet is refracted one way, and the portion falling on the other facet is refracted the other way. The light is thus split into separate channels, and the power in each channel is equal when the star image is exactly centered on the groove.

The light from the separate channels is collected by different portions of a quad lens, and each channel is imaged in a different location on the face of an image dissector. By examining each image in turn with the aperture of the image dissector, the power differential between the channels can be determined and used to generate a null error signal. This is the fine mode of operation.

The particular groove upon which the image falls can be determined by the locations on the image dissector faceplate at which the aperture finds the images. This feature forms the basis of the coarse mode of operation.

Figure 2.0-4 is a schematic of the fine guidance sensor as it is used in the ST.

The entire guide field area for each of the three sensors is covered by a single grating plate, but the field-of-view that can be accommodated by the relay optics in the sensor head is only a small portion of that guide field. Consequently, it is necessary that the sensor head be prepositioned behind the portion of the grating plate where the guide star is expected to appear when the ST is initially pointed via the attitude control system. For this purpose, the sensor head is mounted on a positioning drive system which can be commanded to place the sensor head at the proper location.

FIGURE 2.0-1

FINE GUIDANCE SENSOR FIELDS

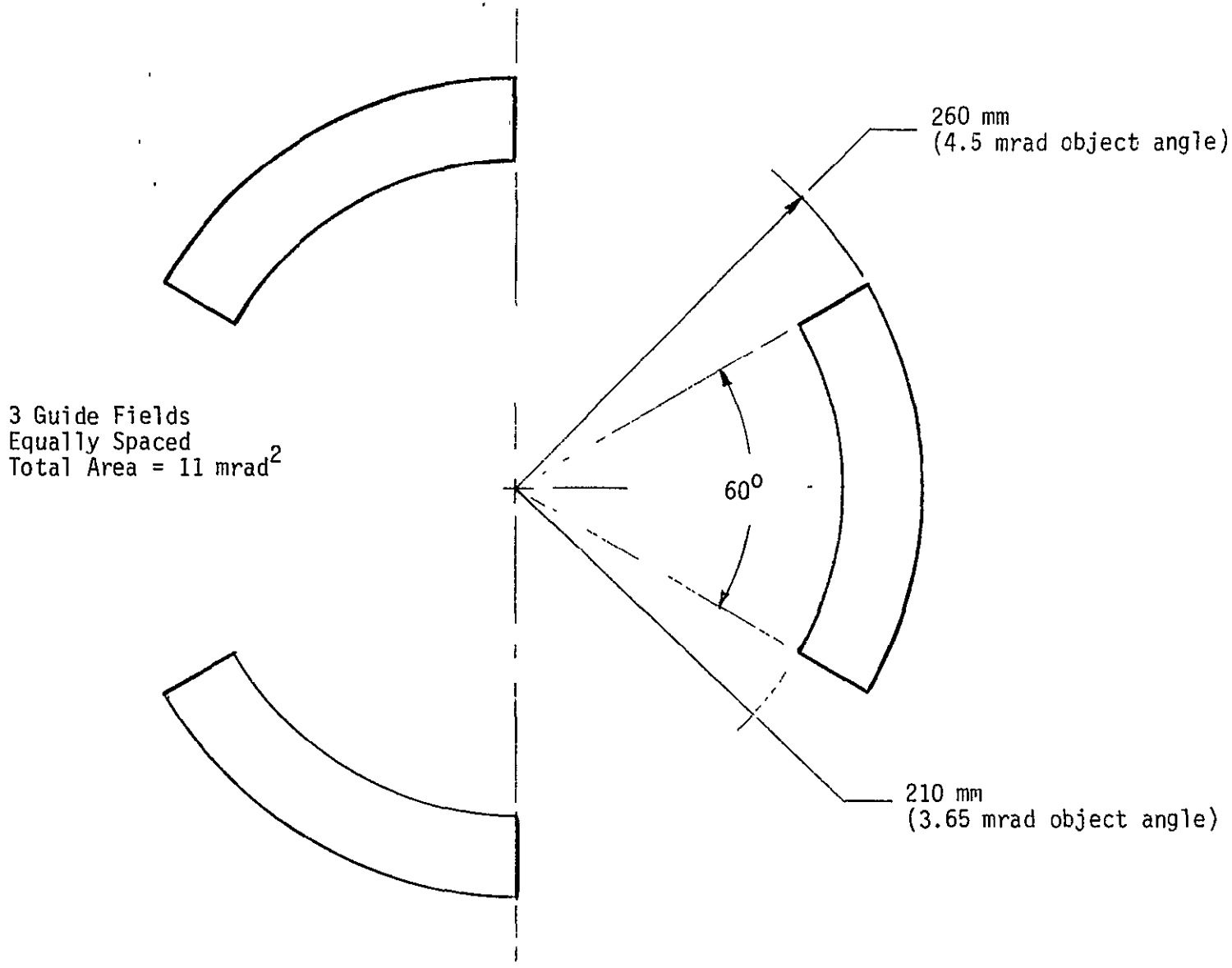

FIGURE 2.0-2

STAR AVAILABILITY

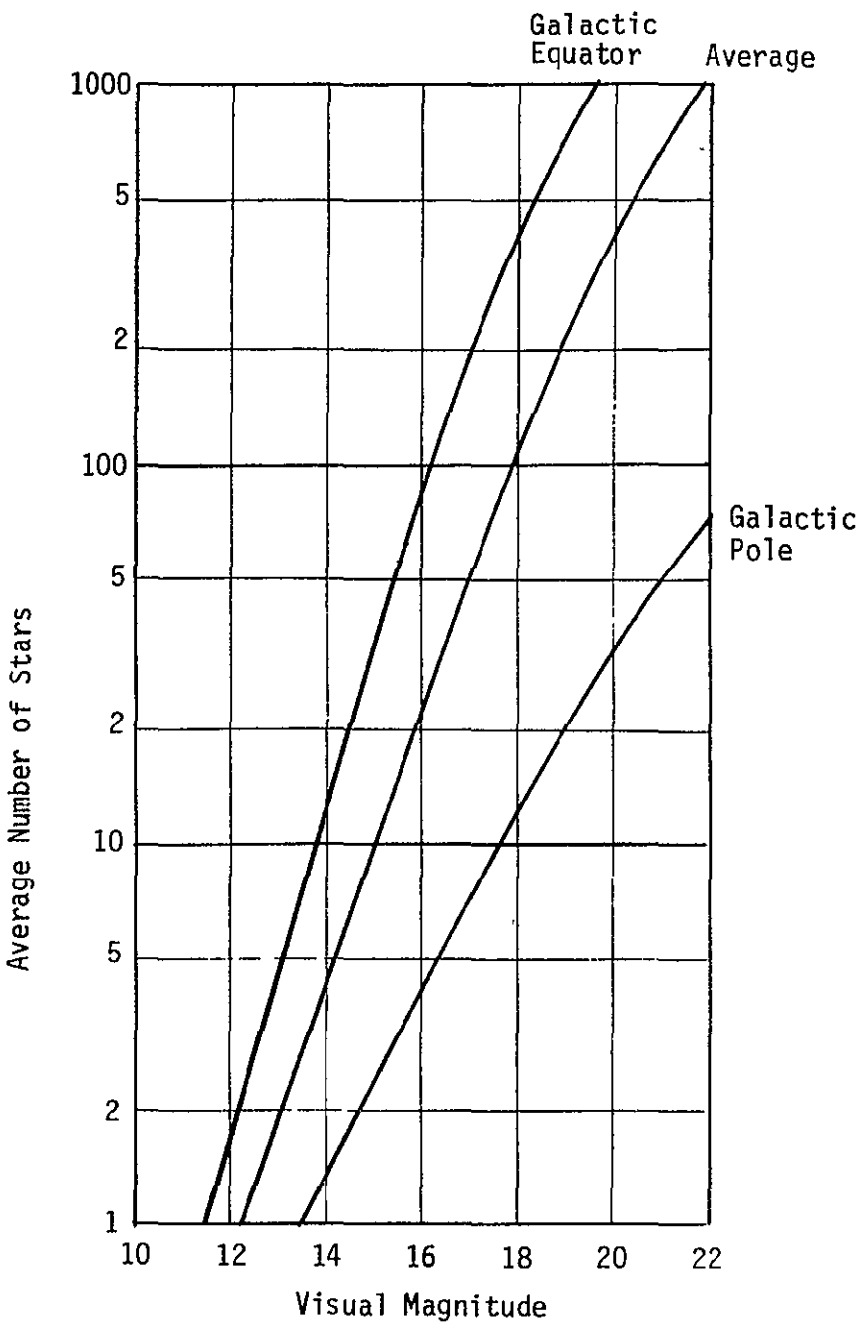

Number of Stars in the 3.7 mrad^2 Field of a Fine Guidance Sensor

FIGURE 2.0-3

OPERATION OF PRISMATIC GRATING SENSOR

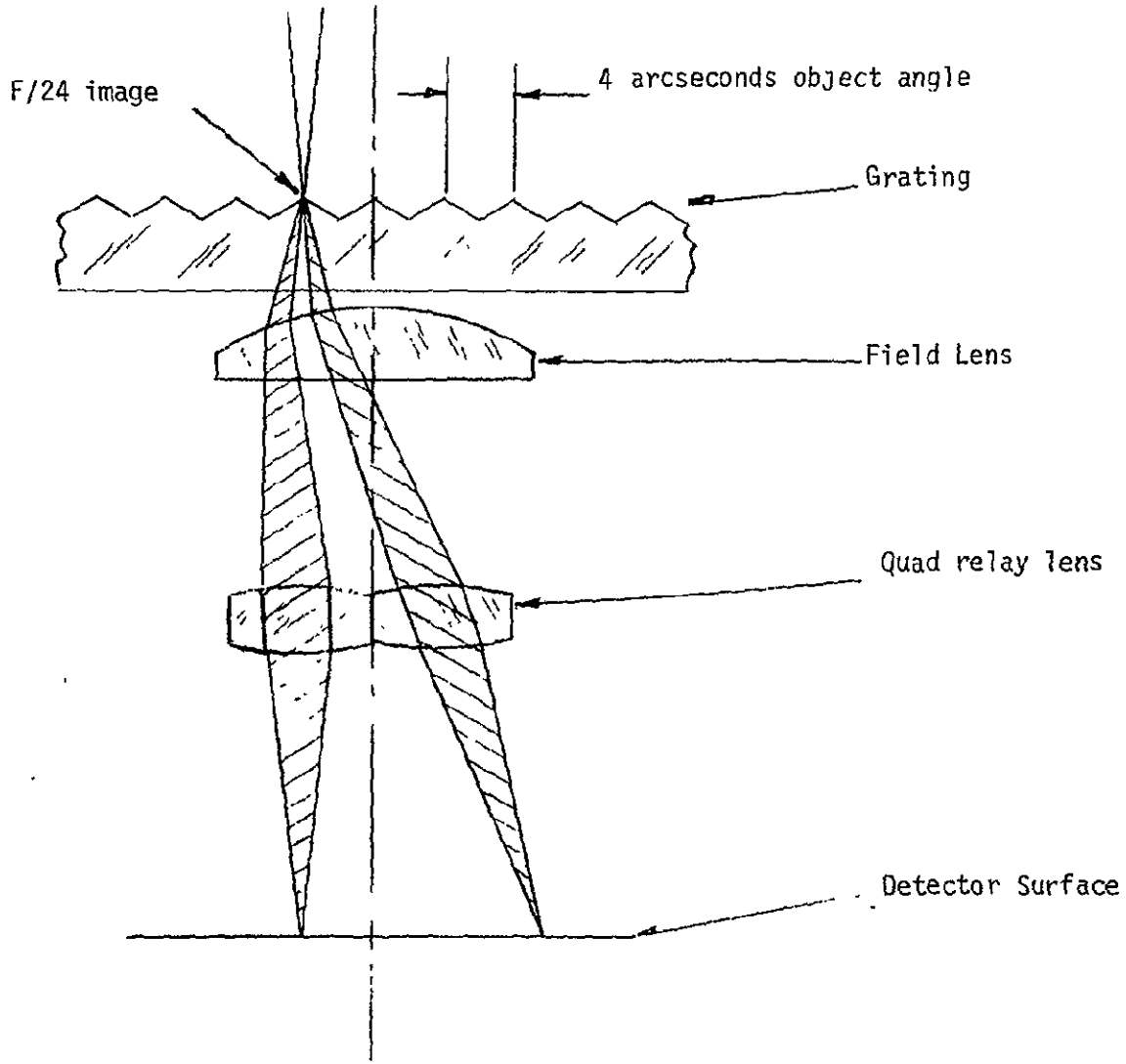

Figure 2.0-4

FINE GUIDANCE SENSOR SCHEMATIC

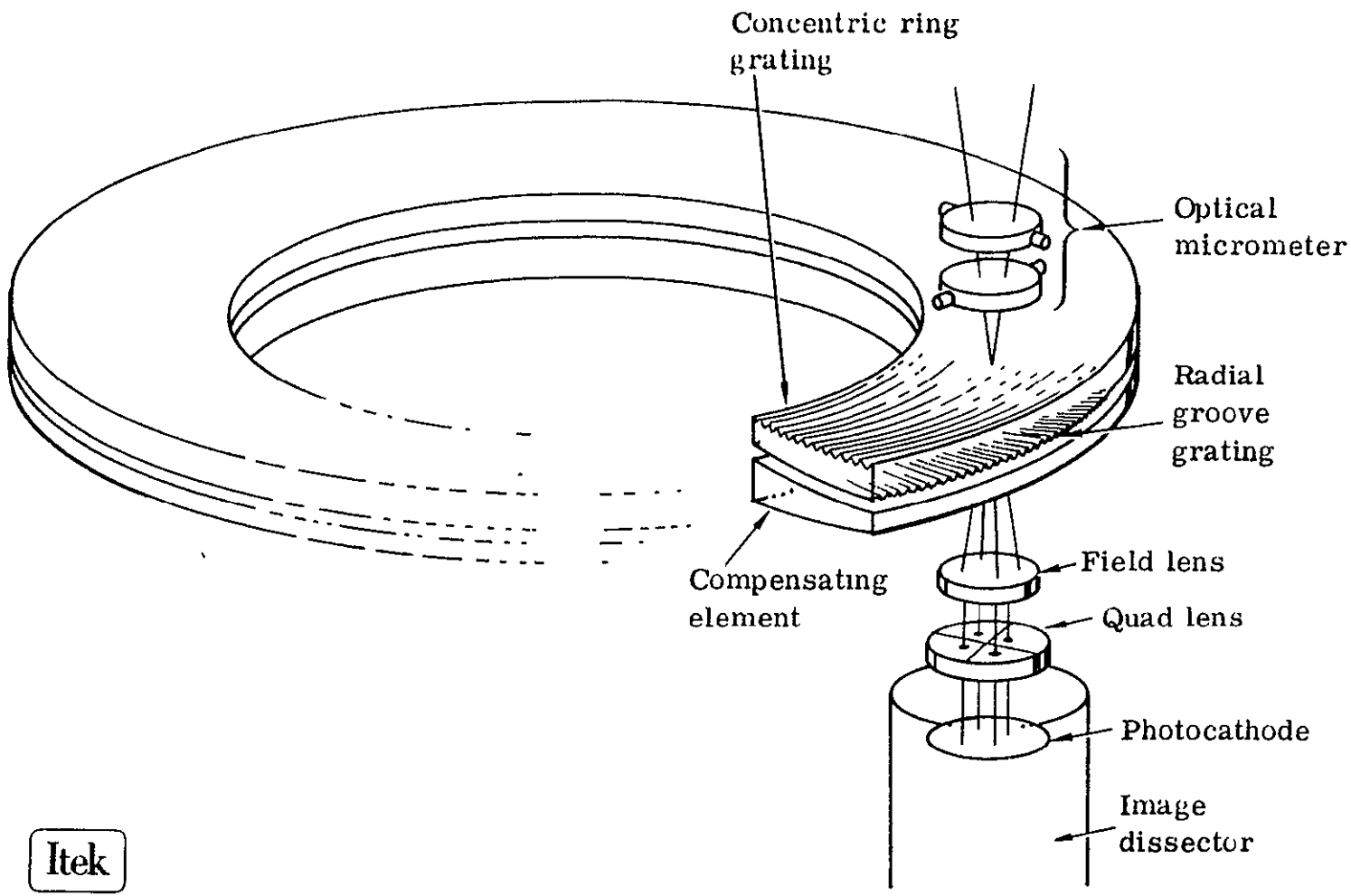

Itek

The converging beam from the guide star is first passed through an optical micrometer, which consists of two gimbaled plane parallel glass plates.

The optical micrometer provides accurately controlled displacements of the guide star image over a range equal to the groove spacing of the grating plate. Since a relatively large angular displacement of each plate produces a small image displacement, the accuracy required of the mechanism is not extreme. By deflecting the micrometer plates appropriately, the fine guidance sensor can fine-track on any guide star image within the field of the reticle grating plate, while keeping the guide star image centered upon a groove intersection.

After the guide star beam has passed through the optical micrometer, it converges to focus at the grating plate. The grating plate is a curved element whose front and rear surfaces conform, respectively, to the tangential and sagittal focal surfaces of the telescope. The grooves on the front surface form concentric rings, since the star image at that surface is blurred tangentially. The grooves at the rear surface run radially since the star image at that surface is blurred in the radial direction. The grating on the front surface divides the light into two beams whose relative power depends upon the radial location of the star image. The grating on the rear surface divides each of the two light beams at that point into two more beams, the relative power of which is dependent upon the tangential position of the star image. This configuration automatically compensates for the astigmatism in the telescope image without the need for additional correctors.

Behind the grating plate is the sensor head, which contains the optical relay elements and the image dissector. The four beams from the guide star image formed by the grating plate are projected onto different points on the image dissector. During fine tracking, the image dissector samples these four beams in sequence, and develops tracking error signals proportional to their differences in power. During initial acquisition, the image dissector also measures the positions of the four beams on the image dissector, and uses this information to provide coarse tracking information. This controls telescope pointing until the guide star image has been brought to the appropriate groove intersection on the grating plate, when fine tracking commences.

The basic astrometric measurement with the fine guidance sensor consists of measuring the angular separation between stars. This is done by making a position measurement of each star individually and then taking the difference of the position measurements to obtain the star separation. Table 2.0-1 lines the measurement sequence.

First, the line-of-sight is stabilized, using two of the three fine guidance sensors, so that the stars to be measured fall within the field of view of the third fine guidance sensor.

The measurement of the position of the first star begins by aligning the sensor head with the grating intersection closest to the star image. This is done from ground determinations of the star position relative to the guide stars to within one arcsecond or so. The sensor will then be ready to go directly to the fine lock-on mode, in which the internal servo loop drives the optical micrometer to null out the fine error signal. At this

point, the star image will have been displaced by the optical micrometer so that it is centered on a grating intersection. The position of the star is then read, using the sensor head position as an indication of the grating intersection, the micrometer angles to determine the vernier distance over which the star image was moved to achieve the null signal, and the fine guidance error signals from the other two fine guidance sensors to account for body pointing error at the time of the measurement.

The position of the second star is then measured by repeating the measurement sequence just described. The separation between the stars is determined by taking the difference between the individual star position measurements.

TABLE 2.0-1

BASIC ASTROMETRIC MEASUREMENT
WITH FINE GUIDANCE SENSOR
(Measure Angular Separation Between Stars)

Stabilize Line-of-Sight Two Stars in Field of Single Sensor	Two Other Fine Guidance Sensors
Measure Position of First Star	
Align Sensor Head With Star Image	ρ Drive θ Drive
Null Fine Mode Signal	Center Image on Grating Intersection With Optical Micrometer
Read Position of Star	Sensor Head Position Micrometer Angles (Vernier) Fine Guidance Error Signal
Measure Position of Second Star Repeat Measurement Sequence	
Determine Star Separation	Difference of Two Position Measurements

For astrometric measurements, the image dissector aperture is centered on the images of the transmitting grating facets so that the grating facets actually define the entrance aperture. The star image, locked on to a grating intersection, appears at the corners of the facets, as shown in Figure 2.0-5.

FIGURE 2.0-5

USE OF IMAGE APERTURE IN ASTROMETRY

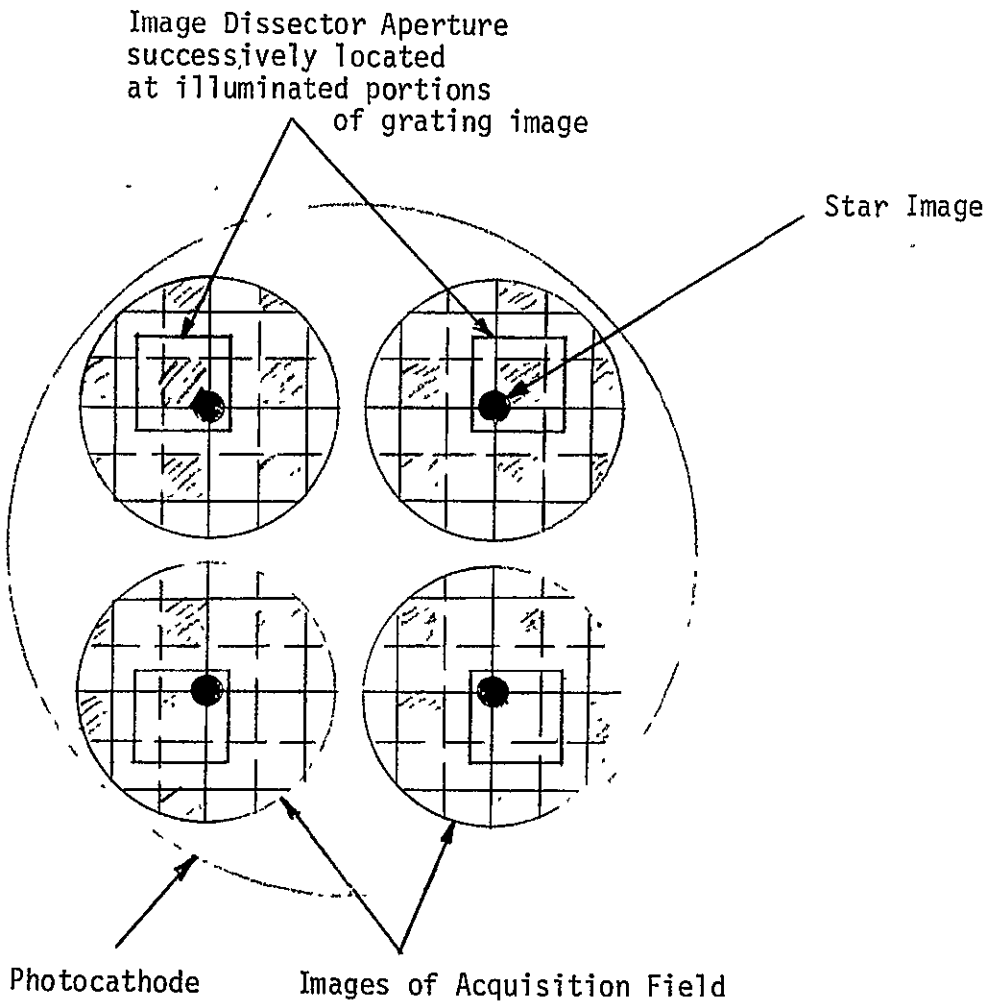

3.0 FINE GUIDANCE SENSOR

Since most of this report deals with the use of the fine guidance sensor for performing astrometric tasks, it is necessary to explain the design and operation of the fine guidance sensor in enough detail so that the reader can then understand how it is used in astrometry. The explanation in this section is intended for such a purpose. For a more detailed description of the fine guidance sensor design, including block diagrams, layout drawings, error analyses, etc., the reader is referred to Volume II B, Optical Telescope Assembly.

3.1 General

Figure 3.1-1 shows an isometric view of one of the fine guidance sensors. The optical micrometer relay, and image dissector are assembled together to constitute the sensor head and can be positioned at the point in the grating at which the guide star is to appear. The field of view of the optical micrometer and relay is large enough to accommodate the 0.3 mrad diametral uncertainty in the initial pointing. Since the gratings are made with circumferentail and radial grooves, the sensor head is positioned by means of a polar coordinate mechanism with its axis of rotation coincident with the axis of the gratings. Thus the sensor head is always rotated to the proper orientation with respect to the gratings, and no additional rotational mechanism is required. Also, the radial motion of the positioning mechanism follows the best straight-line approximation to the curved focal plane of the gratings, which is sufficient to eliminate the need for a separate focusing mechanism.

The grating, which is the only element in the sensor whose positional stability is critical, is mounted to an invar structural bulkhead to which the mounting feet for the instrument are attached. The bulkhead with its mounting feet bridge the hole in the side of the focal plane structure, providing structural continuity for maximum stability of the grating with respect to the scientific instruments mounted to the focal plane housing.

Table 3.1-1 shows the important parameters which characterize the design of the fine guidance sensor. Values are given as they apply to a particular component and in terms of equivalent object space angle.

FIGURE 3.1-1

FINE GUIDANCE SENSOR

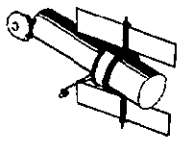

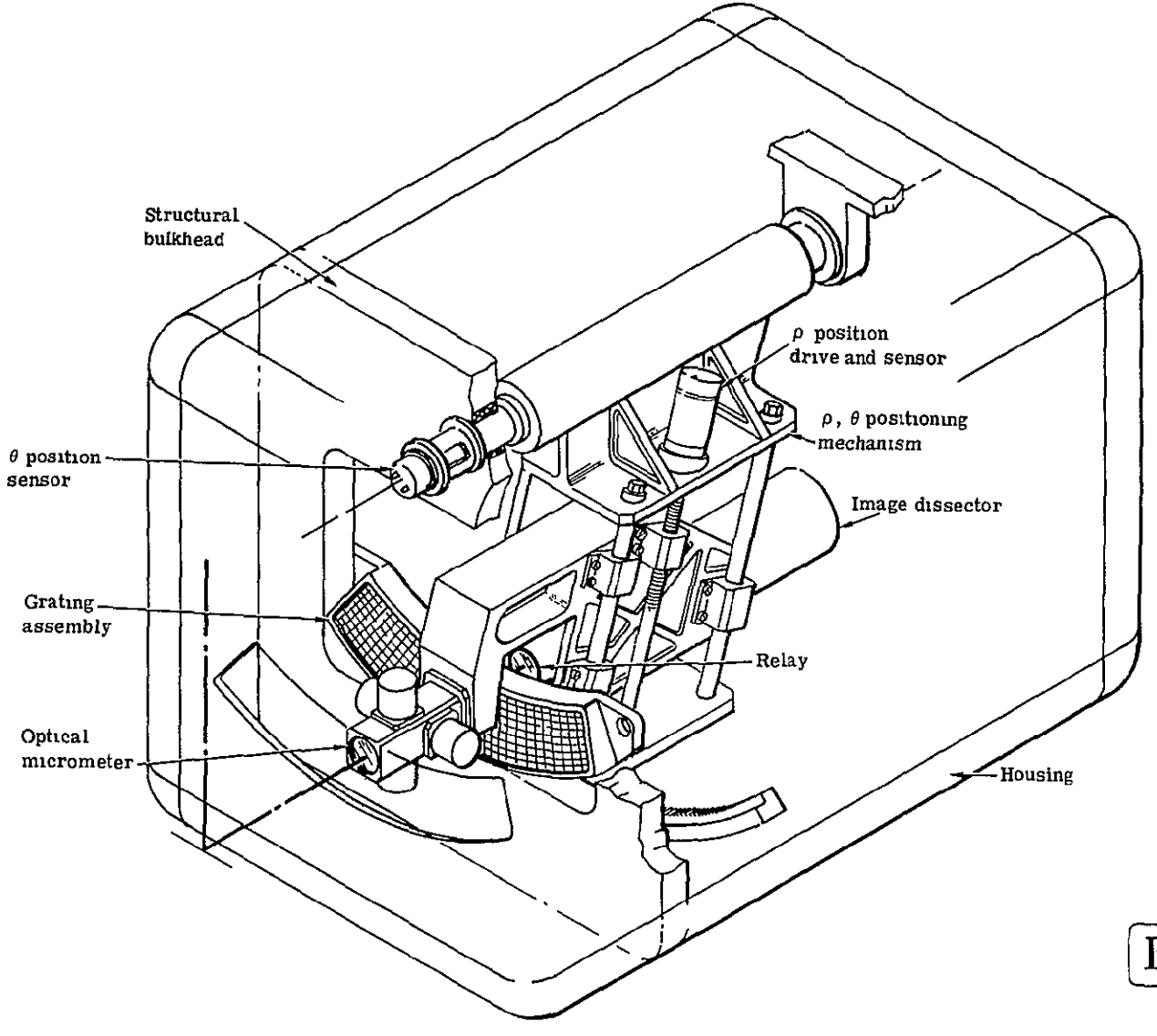

Itek

AV-74-150

TABLE 3.1-1

FINE GUIDANCE SENSOR PARAMETERS

		EQUIVALENT OBJECT SPACE ANGLE
OPTICAL MICROMETER		
Range	± 17°	± 11 μrad
Accuracy	± 15 Arcsec	± 0.0028 μrad
GRATING DIMENSIONS	60° Sector 260 mm max radius 210 mm min radius	3.7 $mrad^2$ each
Spacing		
Circumferential	1.152 mm	20 μrad
Radial	16 arcmin	17-21 μrad
QUAD RELAY ASSEMBLY		
Field of View @ f/24	17.3 mm	0.3 mrad
Reduction	3:1	
IMAGE DISSECTOR		
Photocathode Diameter	25 mm	
Acquisition Field Diameter	5.76 mm	0.3 mrad
Aperture Width	0.38	20 μrad
SENSOR HEAD DRIVE TOLERANCES		
Radial	± 0.05 mm	---
Angular	± 30 arcsec	---
Tip	± 15 arcsec	± 0.0028 μrad

3.2 Grating

A cross section of the plates of the grating assembly is shown in Figure 3.2-1. The circumferential grating is on the first surface of the grating plate, and the radial grating is on the rear surface. Behind this plate is a second plate which compensates for the optical power of the grating plate and causes the center of the four-bundle output of the gratings to be directed parallel to the optical axis so that the exit pupil of the telescope appears at infinity. This permits the sensor head always to remain parallel to the optical axis.

The radii shown are those computed from third-order equations. The focal surfaces are actually parabolic. The gratings can, nevertheless, be made on spheres. For example, the best fit sphere tangent to the circumferential grating at the middle of the field would have a radius of 0.617 M centered 0.6230 ahead of the paraxial image plane on the optical axis. At the outer edge of the field, the focus error would be 0.10 MM, while at the inner edge of the field, the focus error would be 0.000008 MM. This focus error can be reduced virtually to zero by cutting each grating with a radius arm centered not on the optical axis, but in such a manner as to match both the slope and curvature of the parabola. The additional expense involved is that in producing the grating substrate in toric form.

The grating spacing for the circumferential grating is 1.152 MM peak-to-peak which corresponds to 20 microradians object angle. The spacing of the radial grating varies from 1.210 MM at the outer edge to 0.976 MM at the inner edge, the angle between grooves being 16 arcminutes.

The compensating plate behind the grating plate serves to protect the radial grating from dirt. A thin plane parallel window is placed in front of the circumferential grating to protect it.

The grating itself is shown in Figure 3.2-2. The grating is made from a master by replicating in resin on a fused silica substrate. The fused silica substrate provides the dimensional stability required and also permits optical transmission over a wide spectral range. A UV-transmitting resin, index = 1.51, is used in the replication. The masters for the two gratings are ruled with a diamond tool in brass plates. Replication is done with ordinary diffraction-grating technology.

Optical transmission tests conducted at Bausch and Lomb on UV resin 0.006 inch thick showed it to have essentially unity transmission above 4000 Å, and 65% transmission at 3000 Å. Shrinkage of the resin during curing, measured with an interference microscope, was only 0.42 fringe, or about 0.14%.

The master for the circumferential grating most likely would be machined on an existing machine consisting of a turntable and a stationary tool whose position in two directions and tilt can be set under numerical control. A prototype grating was made for Itek by Bausch and Lomb with a machine of this kind.

FIGURE 3.2-1

GRATING ASSEMBLY CROSS SECTION

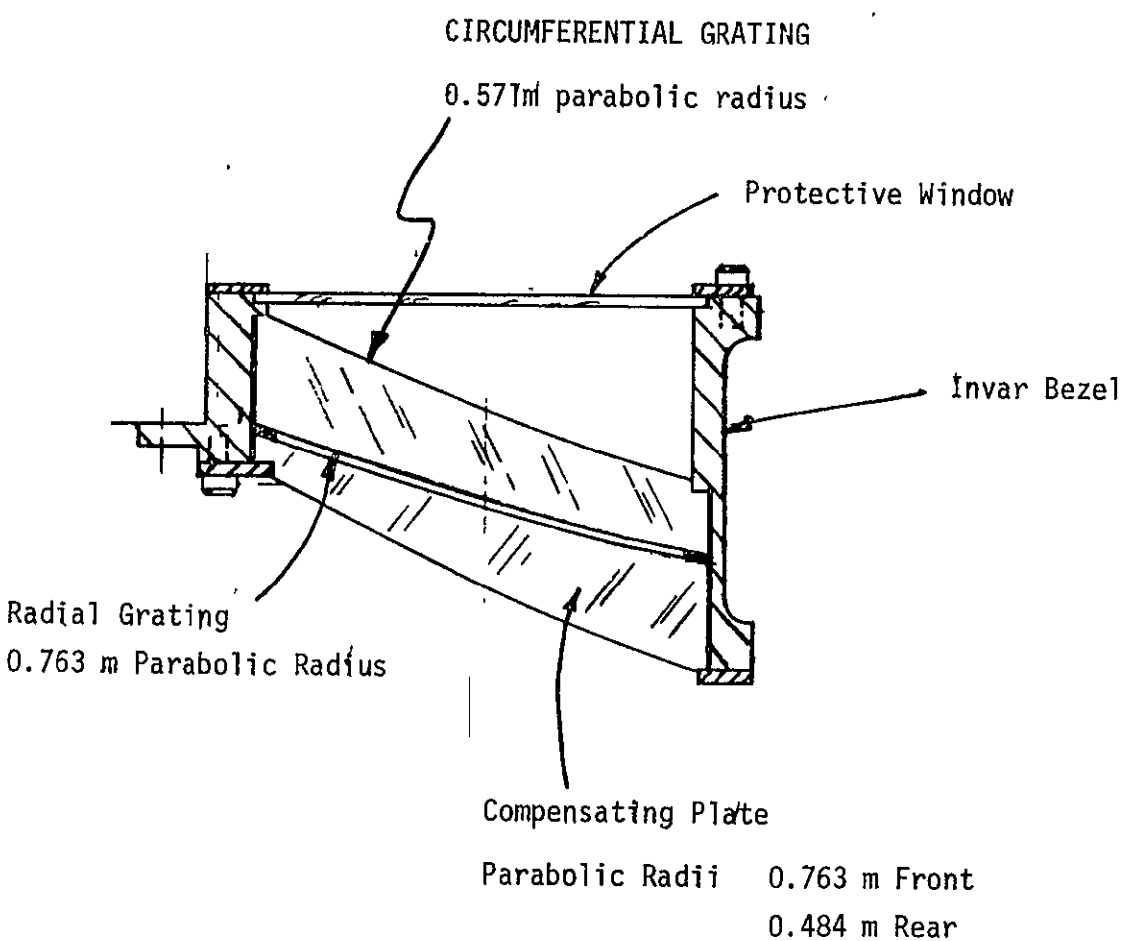

FIGURE 3.2-2

OPTICAL GRATING

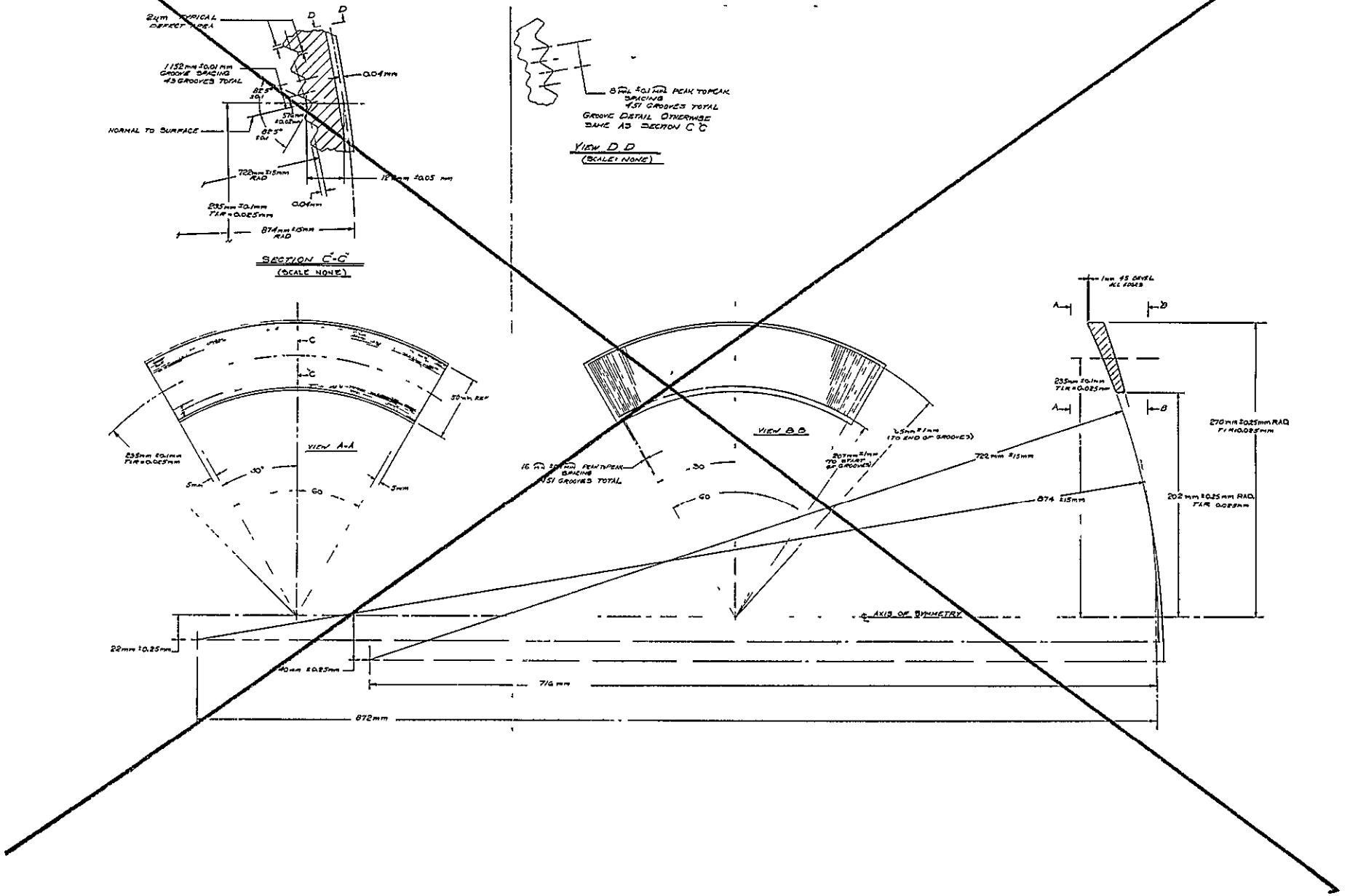

2.

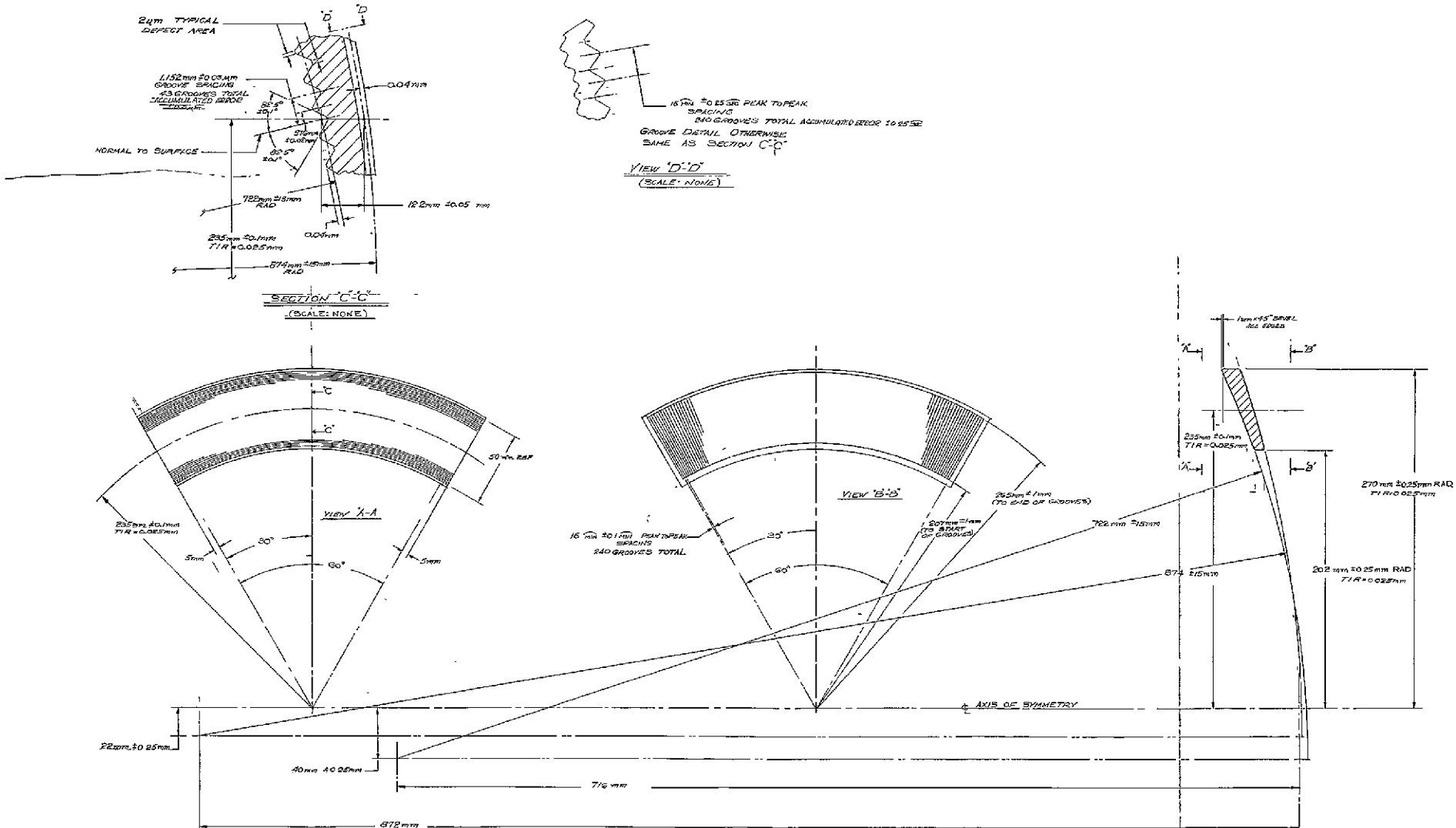

FIGURE 3.2-2

OPTICAL GRATING

FOLDOUT FRAME 2

FOLDOUT FRAME

16a

A91275-J

The master for the radial grating would be machined using a precision pivoted true-radius arm. The 16 arcminute intervals between the grooves would be controlled by a photoelectric microscope sighting on a precision ruled, circular reference scale.

The grating facet angle with respect to the substrate surface is 7.5° to produce beam separation at the relay lens.

Bausch and Lomb indicates that they would make the master blanks identical in size to the product blanks and would assure alignment by carefully matching the outer edges to each other during replication. Special holding and take-apart tooling would be required to protect the first replicated grating while second side is being cemented.

The total thickness tolerance on the grating drawing is 0.100 mm. With any given blank size and a constant viscosity cement, there is a minimum thickness of epoxy resin that the cementer can press out the product blank to. Bausch and Lomb has found that this minimum is very consistent and probably would not vary more than 0.010 mm from product to product. This is the total for both replications. The only problem, then, is to determine the actual resin thickness in this application. To determine the thickness, a test replication is made and the thickness is measured. From this measurement, the proper substrate thickness is determined so that the final product will fall within the blueprint tolerance.

Concerning the stability of the epoxy resin under "space" conditions, Bausch and Lomb relates their experience as follows:

> When BL& first-supplied diffraction gratings for use in orbiting spacecraft, they were all master gratings because of the then unknown performance of our replica gratings under these extreme conditions of temperature and pressure. On one occasion, B&L could not supply the required master in time, and a replica grating was flown. It performed as well as any master that had been used previously. Since then, virtually all space spectrographs have used replica gratings, with no failures.
>
> Most replica gratings for space projects have been supplied on BSC-2 glass which has a linear coefficient of expansion of 71×10^{-7} per degree C.
>
> A significant number have also been furnished as replicas on CerVit and fused silica. In no case has this given rise to any problems because the cement is so thin that it simply follows completely whatever dimension is dictated by the substrate.

3.3 Sensor Head

The items shown in Figure 3.3-1, with the exception of the grating assembly, are part of the fine guidance sensor head which is positioned by a two-stage drive to the point behind the grating at which the guide star image is to appear when the telescope is properly pointed. A capping shutter is included as protection against excessive light levels. It is closed upon receipt of command from the SSM. A filter wheel with six positions, one of which is open, is available to aid in differentiating double stars in performing astrometry.

The optical micrometer is a device that can deflect the guide star image from one peak on the grating to the adjacent peak. The micrometer is designed to have a maximum range in each direction of $\pm$ 11 microradians object angle, which is $\pm$ 634 micrometers deflection of the image at the focal plane. The optical micrometer consists basically, of two plane parallel plates in front of the grating, each 7 mm thick and pivoted so that they can be tipped about orthogonal axes. When the plates are tipped, a lateral shift in the rays passing through is introduced.

Each plate uses a brushless, limited-angle torque motor as a driver and an electromagnetic resolver as the position sensing device. The two devices are located on opposite sides of the plate to minimize crosstalk. The rotary inertia is 0.92 lbm in^2.

Figure 3.3-2 shows the optical micrometer assembly.

RELAY

The grating substrate is made from fused quartz for purposes of dimensional stability. This material is consistent with the desired spectral range, and it is a low chromatic dispersion material, and so it is also the primary material for the rest of the optics.

The basic form of the relay is shown in Figure 3.3-1. It consists of a field lens and four simple reimaging lenses so that the 0.3 mrad acquisition field on the grating is imaged as four separated fields of reduced size on the image dissector photocathode.

The apparent focal plane lies about 10 mm ahead of the rear surface of the compensating plate, so that a 35 mm working distance for the field lens should be adequate. The beam separation chosen is sufficient to accommodate the diffraction effects of the grating.

Details of the design of the optics for the fine guidance sensor have been omitted from this report but are given in Volume IIB - Optical Telescope Assembly, Section 3.5.4. The relay assembly, including the shutter and the filter wheel, is described in Section 3.5.8 of Volume IIB. Several simple modifications to the basic relay compensate for the worst aberrations in the system.

FIGURE 3.3-1

FINE GUIDANCE SENSOR HEAD

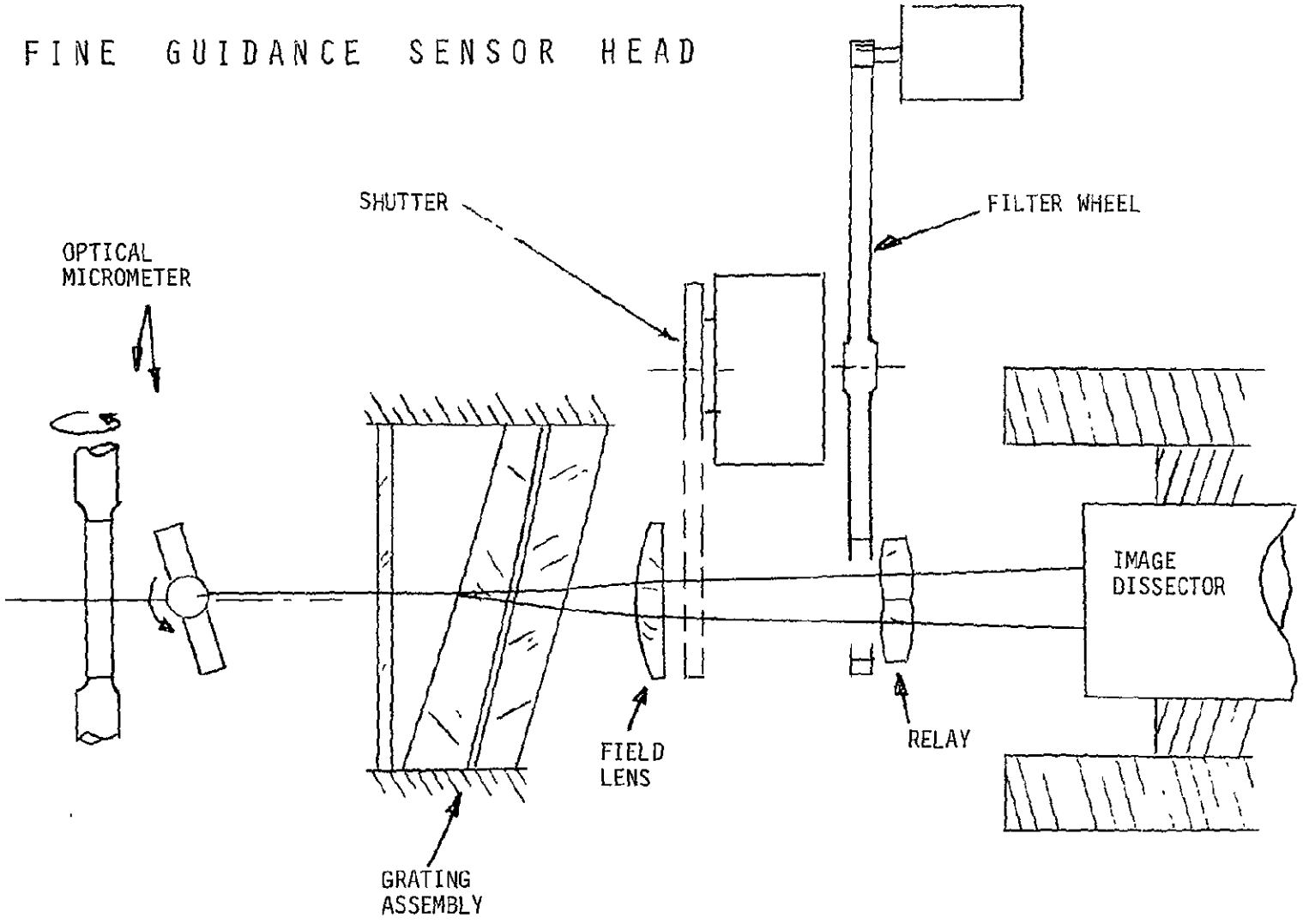

FIGURE 3.3-2

OPTICAL MICROMETER ASSEMBLY

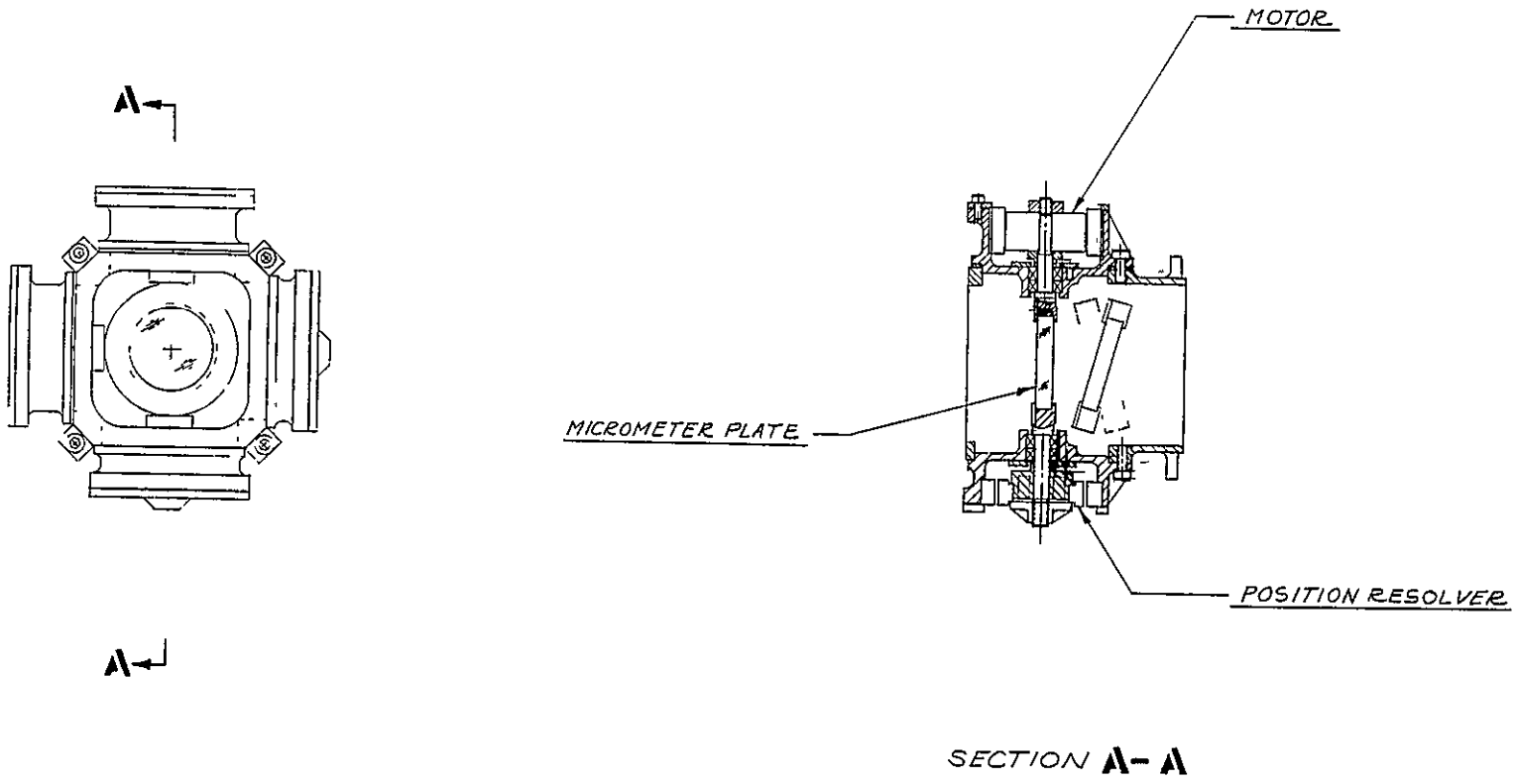

Table 3.3-1 shows the aberrations in their uncorrected form, gives the method of compensation of each and gives the residual image spread after compensation.

The most severe aberrations in the image presented to the image dissector, lateral and longitudinal color and astigmatism, are corrected by several simple modifications to the first order design.

It is desirable to have the optics operate over as broad a spectral range as possible to take full advantage of the spectral sensitivity of the image dissector. An S-20 photocathode has 10% response at about 3000 and 7500 A, and so this spectral range has been used in defining the maximum spot size that must be accommodated by the image dissector aperture.

The sensor head travels in a straight-line approximation to the best focal surface. The result of this is some slight defocus at the center and end positions of the sensor head.

The best focal surface for the relay lies midway between the circumferential and radial gratings. The relay is not normal to this surface, so that at the edge of the acquisition field, the image at the image dissector will not be at optimum focus. This does not matter, however, since only the coarse mode system is in operation until the star image is brought to the center of the field of the relay.

IMAGE DISSECTOR

The image dissector characteristics assumed, based upon an ITT 4011 RP Tube, are given in Table 3.3-2. The photocathode sensitivity of 200 microamps/lumen is available on a selective basis. The aperture uniformity value is derived from R&D work at Itek with a 4011 RP dissector with a 0.6 mm aperture. It tends to have a parabolic form as a function of image position within the aperture.

TABLE 3.3-1

RELAY SYSTEM ABERRATIONS* AND THEIR COMPENSATION

FIELD POSITION	SPOT RADIUS BEFORE COMPENSATION 210 MM	260 MM	METHOD OF COMPENSATION	MAXIMUM RESIDUAL AFTER COMPENSATION OF MEAN
LATERAL COLOR (3000-7500 Å)				
Tipped Plane Parallel Plate Effect of Grating and Compensator	0.25 MM	0.31 MM	Wedge in Relay, Tip of Detector	0.030 MM
Deflection in Field Lens	0.034 MM	0.034 MM	Decenter of Relay	0.00 MM
LONGITUDINAL COLOR IN GRATING, COMPENSATOR, FIELD LENS, AND RELAY (3000-7500 Å)	0.21 MM	0.21 MM	Achromatic Relay	0.01 MM
ASTIGMATISM IN TELESCOPE RELAY AND RELAY	0.07 MM	0.10 MM	Astigmatic Relay	0.018 MM
DEFOCUS FROM STRAIGHT LINE APPROXIMATION OF FOCAL PLANE	—	—	—	0.010 MM

*Aberrations given in terms of spot radius at F/24

TABLE 3.3-2

IMAGE DISSECTOR CHARACTERISTICS
(Based upon ITT 4011 RP)

Photocathode Quality Diameter	21 mm (0.825 inch)
Photocathode Sensitivity (Selective Basis)	200 a/Lumen
Output Uniformity	90 ± 10% over photocathode quality diameter
Aperture Collection Efficiency	65% of photoelectrons emitted by photocathode
Aperture Uniformity (Parabolic)	95 ± 5% variation over aperture area
Aperture Width	0.384 mm (0.015 inch)

3.4 Aperture Centering

The size of the image dissector must be consistent with the image spot size at the aperture and the accuracy with which the relative positions of the image and the deflected aperture are known.

The image size seen by the image dissector is determined from the diffraction spot, the aberrations, and the image dissector electron optics. These sources of image growth are summed up in Table 3.4-1. More than 96% of the energy will fall within the direct sum radius, whereas the effective spot diameter is better represented by the RSS value.

The aperture is sized to have twice the width of a grating facet. It is square with a 0.384 mm width, equivalent to 1.152 mm at f/24. Since in each of the four images of the grating on the image dissector photocathode only one out of every four facets is illuminated, the aperture can be centered on a given facet and receive light through that facet only. In this case, it is the grating facets and not the image dissector aperture that acts as the field stop in the system.

Uncertainties in the position of the aperture relative to the facet give a maximum relative location error as shown in Table 3.4-2.

TABLE 3.4-1

IMAGE SIZE SEEN BY IMAGE DISSECTOR
(Images Projected Back to F/24 Focal Plane)

	IMAGE RADIUS AT F/24, MM	
	96%	RSS
DIFFRACTION SPOT		
7 Airy Radii (96% encircled energy)	0.11	
1 Airy Radius (effective spot size)		0.02
ASTIGMATISM AND DEFOCUS	0.035	0.035
Optical Micrometer 0.017 mm		
Telescope and Relay 0.028 mm		
COLOR SMEAR (3000-7500 Å)		
Optical Micrometer	0.02	0.02
Grating and Relay	0.04	0.04
IMAGE DISSECTOR	0.075	0.075
(0.025 mm Rise Distance at F/8)		
DIRECT SUM (most of energy)	0.28 mm	
RSS (effective spot size)		0.10

TABLE 3.4-2

IMAGE DISSECTOR APERTURE POSITION ERRORS

	RADIUS AT F/24, MM
SENSOR HEAD POSITIONING (± 0.05 mm)	0.05
SENSOR HEAD TILT (± 15 Arcsec)	0.01
DEFLECTION STABILITY (1/500 over 18 mm at F/8)	0.11
QUANTIZATION (10 Bits)	0.02
CALIBRATION OF ALIGNMENT	0.006
EARTH'S MAGNETIC FIELD (1000/1 Shielding)	0.006
DIRECT SUM	0.20
RSS	0.12

The image size is shown in Figure 3.4-1 for a star at a grating intersection (the corner of a facet). As is indicated in the figure, the image dissector positioning accuracy is sufficient to assure collecting the greatest portion of the light from the star in the acquisition mode. Greater accuracy in positioning the aperture is required for astrometric measurements however.

An automatic deflection calibration routine is one of the operational sequences available and this routine is used after acquisition for each star whose position is to be measured.

After lock-on to a star is achieved in the fine mode, and the star image appears in all four of the image fields on the face of the image dissector, initiation of the calibration routine causes the image dissector aperture to nutate about the image in each quadrant to develop a deflection error signal. This calibration sequence is illustrated in Figure 3.4.2. The nutation pattern is a four-position pattern with the four corners of the aperture successively centered on the star. If the nutation pattern in a given quadrant is not exactly centered upon the star image, then the image dissector will detect an energy imbalance signal modulated at the nutation frequency. The signal is demodulated to derive a deflection correction signal for the average deflection, or centroid, of the nutation pattern. The average deflection is corrected so that equal energy is admitted to the aperture in each of the four nutation positions, at which point, the corrected average deflection for that image field is used to update the deflection command. After the deflection commands for all four image field are corrected, the calibration routine is terminated.

3.5 Optical Transfer Function

In determining the photon noise contribution to stabilization error, it is necessary to know the optical transfer function from pointing error to differential photon count rate in the four photon counting channels in the image dissector electronics. This transfer function has been computed for the telescope, taking into account the aperture and the focal ratio, the central aperture obscuration, the wavefront aberrations introduced by the telescope mirrors, the expected defocus, and the slight aberrations introduced by the optical micrometer over its normal range of travel.

The optical micrometer introduces aberrations into the image when its plates are tipped to displace the image laterally. The aberrations are primarily lateral color, astigmatism, and defocus. The amounts of the aberrations are functions of the micrometer deflection.

One of the aberrations introduced by the optical micrometer with the plates tipped is lateral chromatic smear. Chromatic smear is like image motion smear except that the RMS smear produced is the dispersion at the RMS spectral bandwidth of the sensor. An S-20 photocathode response with the centroid and RMS value is shown in Figure 3.5-1. The RMS value is about 1000 Å so that the equivalent RMS image motion is the color smear associated with a $\pm$ 1000 Å band, or about 4000-6000 Å.

FIGURE 3.4-1

IMAGE SEEN BY IMAGE DISSECTOR

(Aperture and Image Projected Back to F/24 Focal Plane)

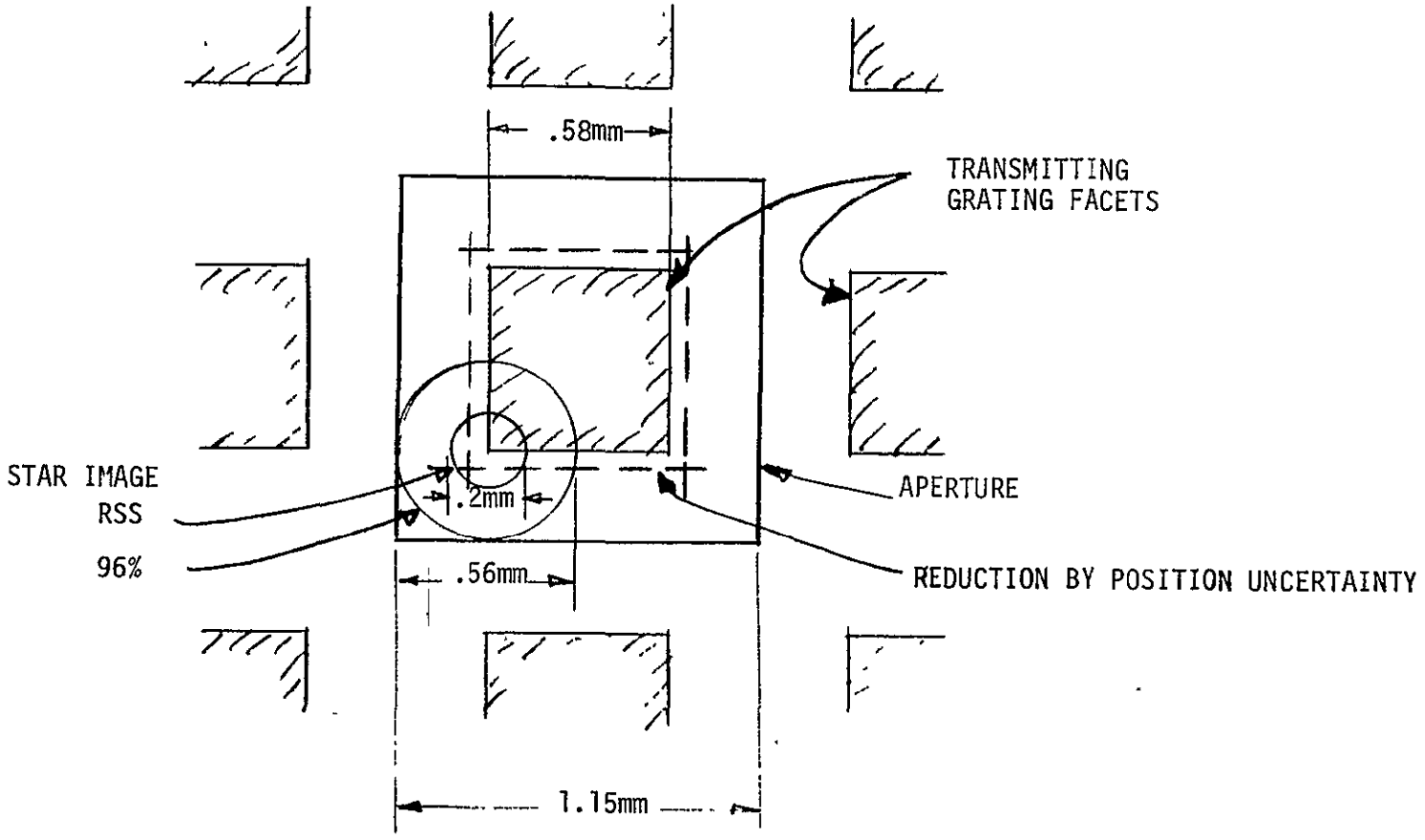

FIGURE 3.4-2

CALIBRATION OF IMAGE DISSECTOR DEFLECTION

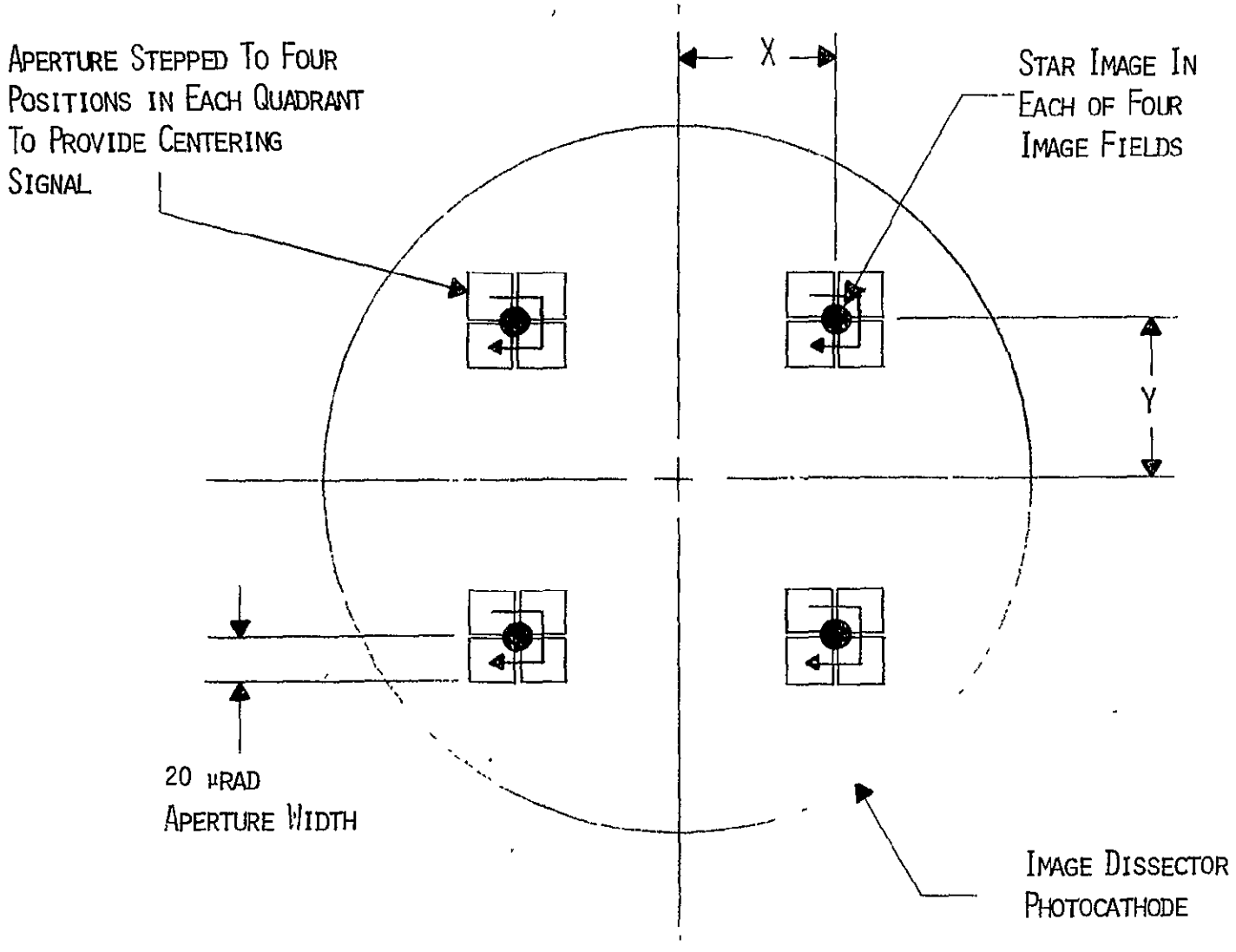

FIGURE 3.5-1

S-20 PHOTOCATHODE RESPONSE

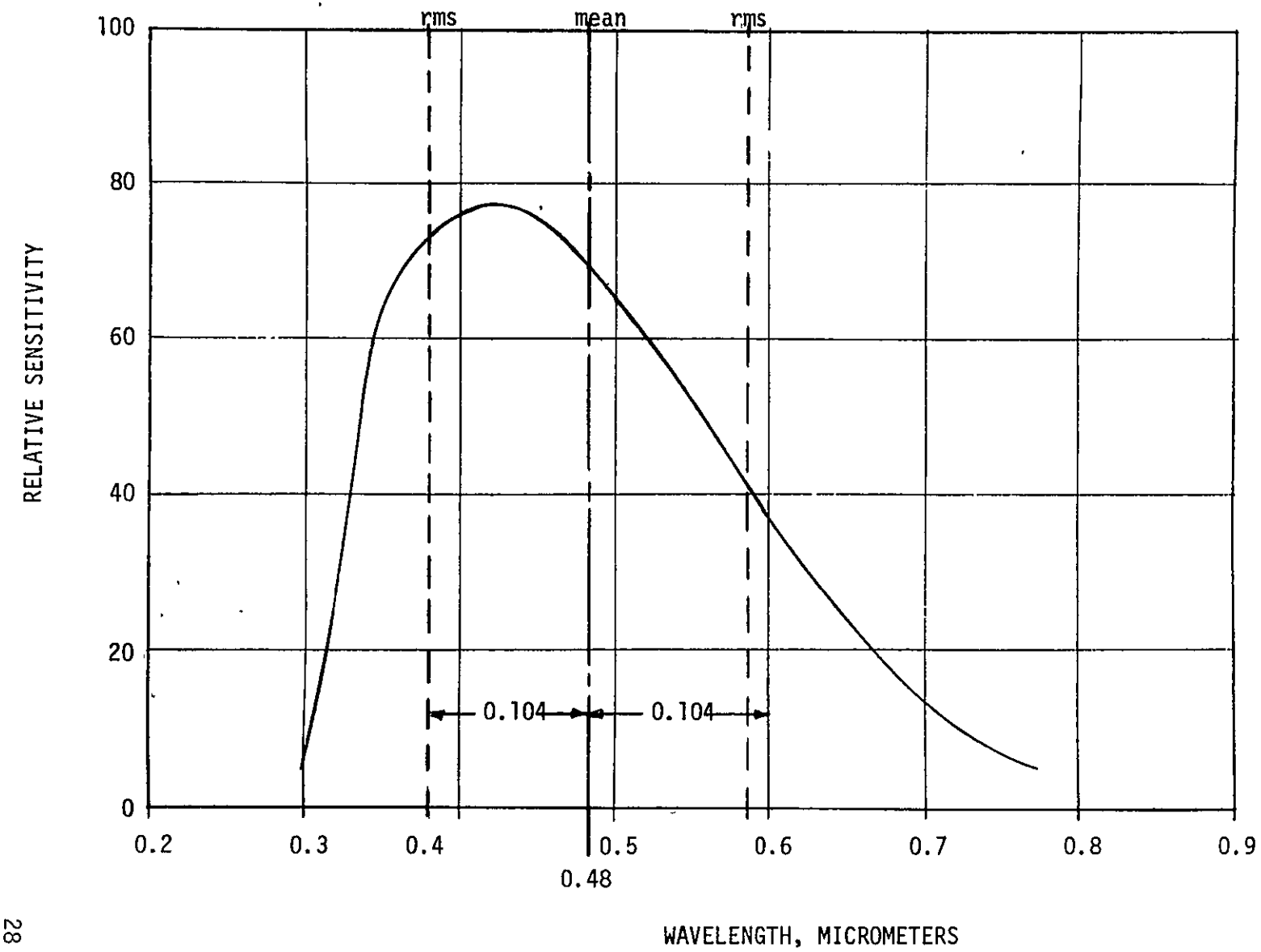

To predict the fine guidance sensor performance at various micrometer deflection positions, the micrometer aberrations were added to the expected OTA aberrations so that the overall image quality could be computed. The OTA aberrations assumed were 0.055 waves RMS random wavefront error at 0.6 micrometer, with a correlation distance of 30% of the telescope aperture. Defocus of the OTA of 220 micrometers at the focal plane (corresponding to about 0.02 waves RMS) was assumed. Image smear of 2 micrometers RMS (0.007 arcseconds RMS) was assumed. To these values were added the effects of the micrometer defocus and astigmatism and lateral color smear for line-of-sight deflections of 5 microradians and 10 microradians. Table 3.5-1 shows the resulting telescope aberration characterization as a function of image displacement introduced by the optical micrometer.

Another aberration, coma, is negligibly small. At the maximum line-of-sight deflection of 10 microradians, the coma spot size is only 0.6 micrometer (0.002 arcsecond).

TABLE 3.5-1

TELESCOPE ABERRATION CHARACTERIZATION AS FUNCTION OF OPTICAL MICROMETER DEFLECTION

LOS DEFLECTION	0	5 μRAD	10 μRAD
WAVEFRONT ERROR (λ = 0.6 M)	0.055 RMS	0.05 RMS	0.05 RMS
DEFOCUS AND ASTIGMATISM (Longitudinal)	220 μM	380 μM	620 μM
LATERAL SMEAR	2 μM_{RMS}	3.9 μM_{RMS}	6.9 μM_{RMS}

Edge response functions computed for OTA with optical micrometer aberrations added are shown in Figure 3.5-2.

The effective image width used in sensitivity calculations is the reciprocal of the peak slope of the edge function. For normal stabilization, the micrometer never deflects beyond $\pm$ 5 microradians, so that the largest image width normally encountered is 24 micrometers. For solar system observations, in which the telescope must be stabilized non-inertially, and in astrometry using scanning by the micrometer, the optical micrometer may be used over its full range, so that the maximum image width encountered will be 33 micrometers.

The effective image width, defined as the reciprocal of the maximum slope of the edge spread function, is shown in Figure 3.5-3 for the image at the grating as a function of the line-of-sight deflection introduced by the optical micrometer.

FIGURE 3.5-2

EDGE SPREAD FUNCTION OF IMAGE AT GRATING

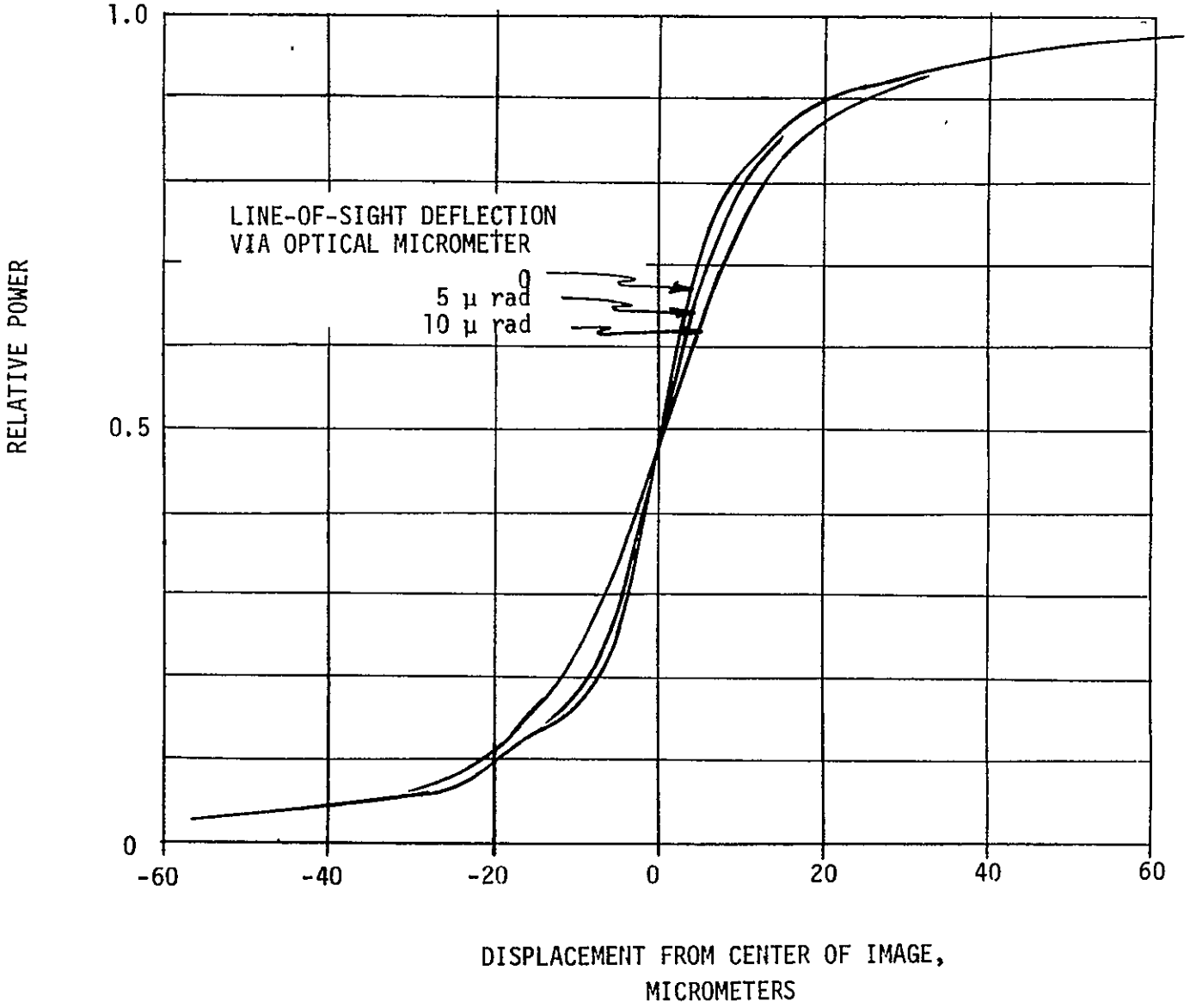

FIGURE 3.5-3

SYSTEM IMAGE WIDTH VS. OPTICAL MICROMETER DEFLECTION

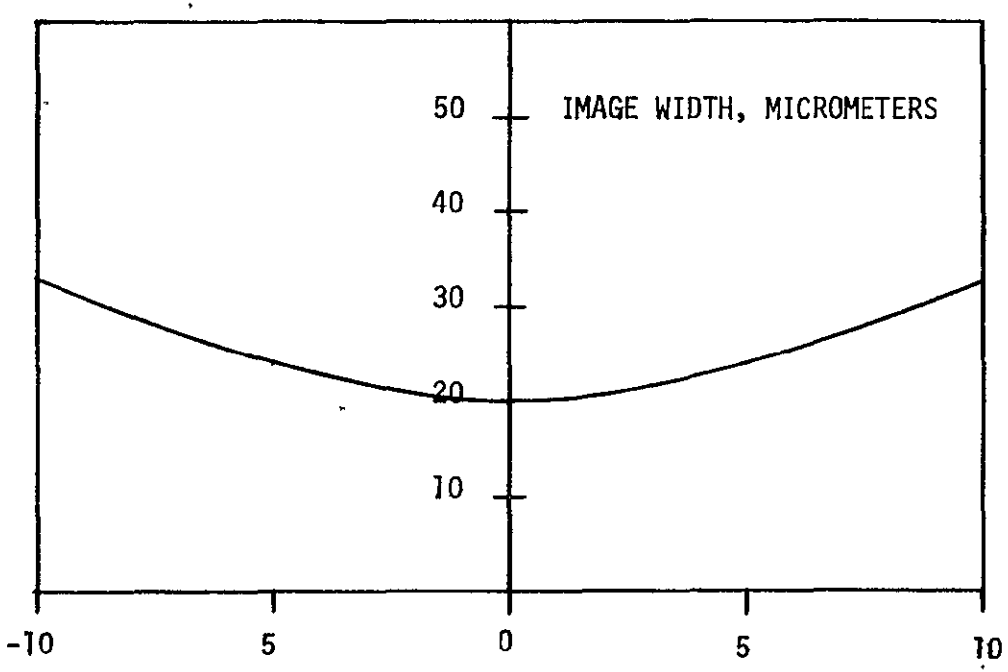

LINE-OF-SIGHT DEFLECTION VIA MICROMETER
MICRORADIANS

3.6 Stabilization Errors

The photoelectron rate expected from a M_V13, Class G3 star, based upon a 2.4 meter collecting aperture and an S-20 photocathode with a 200 microamp/lumen sensitivity, is 94,400 photoelectrons/second. The estimated optical transmission is 37%. An image dissector collection efficiency combined with the photoelectron counting efficiency is estimated to be about 58%. A duty cycle of 25% applies since the four optical channels are sampled sequentially. The estimated photoelectron rate is then, 5100/second. This is used as the basis of the subsequent noise analysis.

The effective image width for the $\pm$ 5 microradians normal maximum optical micrometer deflections is 24 micrometers or about 0.42 microradians in image space.

The RMS sensor noise equivalent blur is: $0.42\ \mu rad/2\sqrt{N}$; where N is the number of photoelectron counts within the effective integration interval. Figure 3.6-1 shows this function evaluated as a function of visual stellar magnitudes for several effective integration times. Over the range of magnitudes shown in Figure 3.6-1, the sensor performance is limited by the photon noise from the star.

The astronomical background in earth orbit is made up of diffuse sunlight scattered by debris in the solar system and of other stars dimmer than the guide star. The scattered sunlight is a function of pointing angle with respect to the sun and will be equivalent to a star of visual magnitude 22.2 to 19.1 when viewing 45° from the sun.

The dark current for the S-20 photocathode at 70°F will be on the order of 10^3 counts/second/cm^2 (see the HRC FID). The aperture has an area of 0.0015 cm^2, and so the dark count will be on the order of 1.5 counts per second.

Anode leakage produces a finite current owing to the high voltage gradient between the anode pin and lower voltage pins nearby. The leakage is probably due to surface leakage along the glass and is accentuated by contaminants on the surface. Typical amounts are 10^{-10} to 10^{-9} ampere. The noise in it though, is several orders of magnitude less than the peak current and is many orders of magnitude smaller than the individual photoelectron pulses (about 10^{-6} ampere for bandwidth = 10^7 Hz and gain = 10^6).

It is clear that by selecting the photon counting mode of operation, sources of noise other than shot noise in the signal current may be made negligible compared to the counts received from the guide star, so that the system is virtually limited only by the photon noise of the guide star.

Predicted guidance sensor errors, including the photoelectron noise and other errors, are given in Table 3.6-1.

FIGURE 3.6-1

PHOTON NOISE OF FINE GUIDANCE SENSOR AT VARIOUS INTEGRATION TIMES

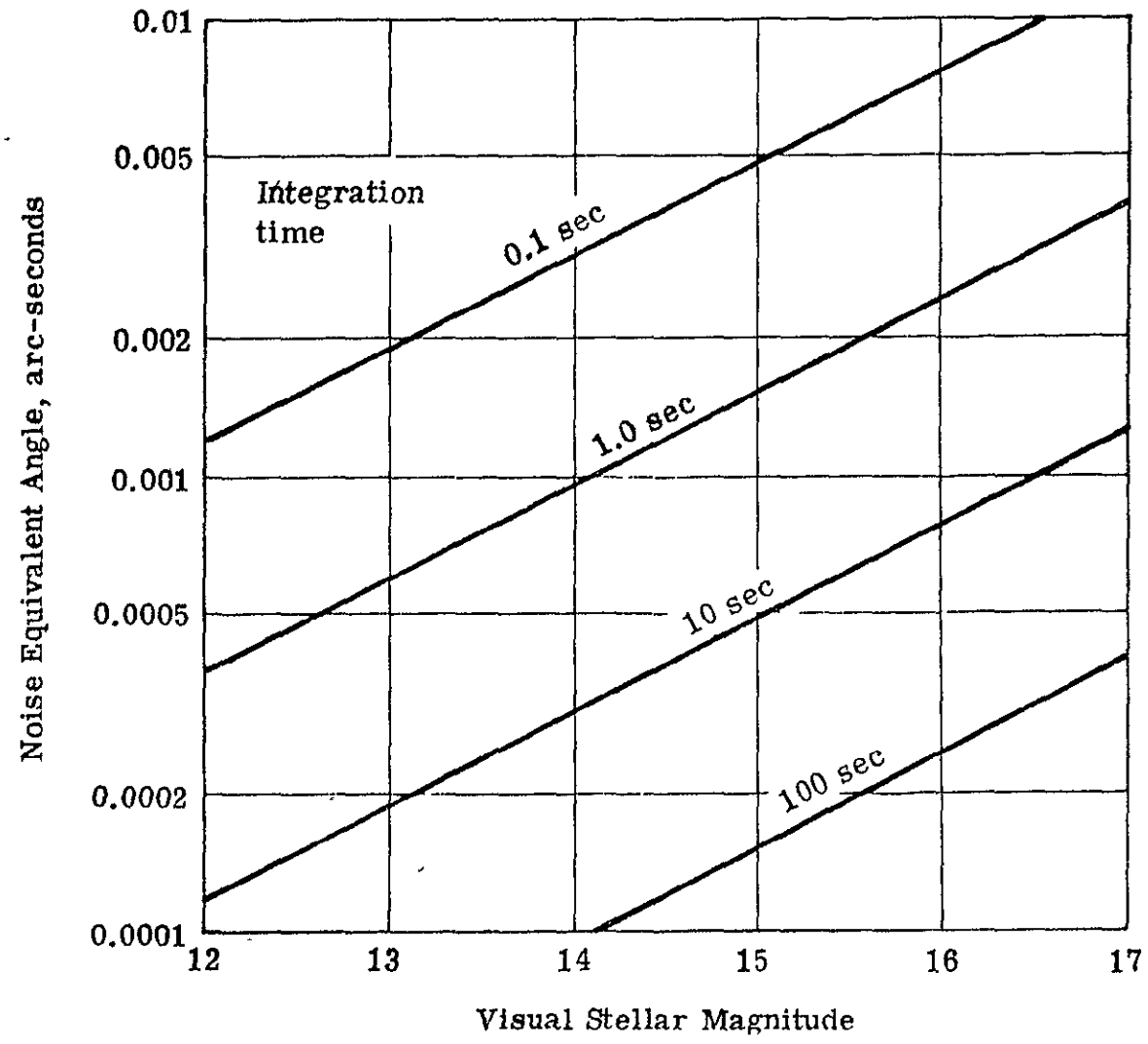

TABLE 3.6-1

GUIDANCE SENSOR STABILIZATION ERRORS

		LINE-OF-SIGHT ERROR MICRORAD. (ARCSEC.)
SENSOR PHOTOELECTRON NOISE (5 Hz Noise Equivalent Bandwidth, M_V 13.3 Star)		0.010 (0.0021)
BANDWIDTH-INDEPENDENT ERRORS (RSS)		0.0053 (0.0011)
Quantization (13 Bits)	± 0.0014	
Optical Micrometer Resolver (± 15 Arcsec at Axis of Rotation)	± 0.0028	
Optical Micrometer Mount (± 15 Arcsec Tip)	± 0.0028	
Image Dissector Aperture Drift	± 0.0025	
Gyro Roll Error	± 0.002	
Body Point Command	± 0.0008	
RSS ERROR		0.011 (0.0023)
ALLOWABLE		0.017 (0.0035)

The image dissector aperture drift results in an error because of the variation of the sensitivity over the width of the aperture. Assuming a 10% variation over the aperture in parabolic form gives a 0.6% power balance change. This is the result of the differential drift of the apertures at the four image locations equal to a predicted 0.2 mm maximum. The power balance change, coupled with the 24 micrometer image width gives the 0.14 micrometer error at the focal plane. This is equivalent to the 0.0025 microradian line-of-sight error in the error budget.

The only effect of varying magnetic fields upon stabilization comes through the aperture nonuniformity phenomenon, and the effect is included in the aperture position uncertainties.

The optical micrometer mount error is the result of the sensor head, upon which the micrometer is mounted, tipping by its 15 arcsecond allowable tip during an observation. The body point command error is the result of the 10 millisecond sampling interval.

One error there, which is not from the sensor itself, is the gyro roll error. If an assumption is made that the second guide star is significantly dimmer than the primary guide star, but that the second fine guidance sensor is operated with an integration time such that the error level is the same as for the first, then, over a long period of time, the two sensors will actually reinforce each other to reduce the RMS error. Over a shorter duration, however, say in the 0.1 to 5 Hz bandwidth range, the roll error signal must come from the SSM reference gyros. Assuming a gyro error of 0.1 arcsecond over this time interval, that error multiplied by the ST 0.004 radian half field angle gives a 0.002 microradian error.

The RSS error is 0.012 microradian (0.0025 arcsecond). This compares to an allowable error of 0.017 microradian (0.0035 arcsecond), which is based upon an equal partition of the 0.034 microradian (0.007 arcsecond) OTA error requirement between the fine guidance sensor, body pointing error, vibration, and thermally-induced dimensional changes within the OTA.

3.7 Dynamic Disturbances

Each fine guidance sensor contains moving parts which may be in motion during scientific observations. Both the sensor head and the optical micrometer are moved for solar system observation and for astrometry.

The tolerable body disturbance depends upon the body stabilization control system and the time duration of the disturbance. A gain crossover frequency of 3 rad/second (0.5 Hz) was assumed.

The vehicle inertia used was 121 x 10^6 lbm in.^{2}; the sensor head mass is 20 lbm at 41 inches from the vehicle center-of-gravity, the flywheel inertia is 3.86 lbm in.^{2}, and the micrometer inertia is 0.92 lbm in.^{2}. The allowable line-of-sight error used was 0.005 microradian.

Analysis showed that a limited-jerk motion profile is required. Figure 3.7-1 shows the form of the sensor head motion profile to be generated by the FGS that meet the limited-jerk requirements. It turns out that it is the motion of the sensor head that must be limited to a jerk value of 0.00066 in/sec^3. The flywheel motion corresponding to this is 0.041 rad/sec^3, and the corresponding time to move the sensor head the full 10-inch distance across the grating is 80 seconds. The maximum velocity achieved will be 0.25 inch/second.

The time it takes to move the sensor head over a given distance, in terms of object space angle, works out to be:

$$T(\text{seconds}) = 4.8\ \Delta\theta^{\,1/3}\ (\text{microradians})$$

This function is shown graphically in Figure 3.7-2.

M_V 17 stars will, on the average, be separated by about 0.3 millirad (1'), so the average time required to move the sensor head will be about 32 seconds.

Line-of-sight disturbances to the instruments from motion irregularities of the fine guidance sensor head, including body pointing and elastic body disturbances, were calculated. The elastic body disturbances were calculated using a preliminary dynamics model of the SI area structure.

FIGURE 3.7-1

MOTION PROFILES TO MOVE
SENSOR HEAD
FROM ONE POSITION TO ANOTHER

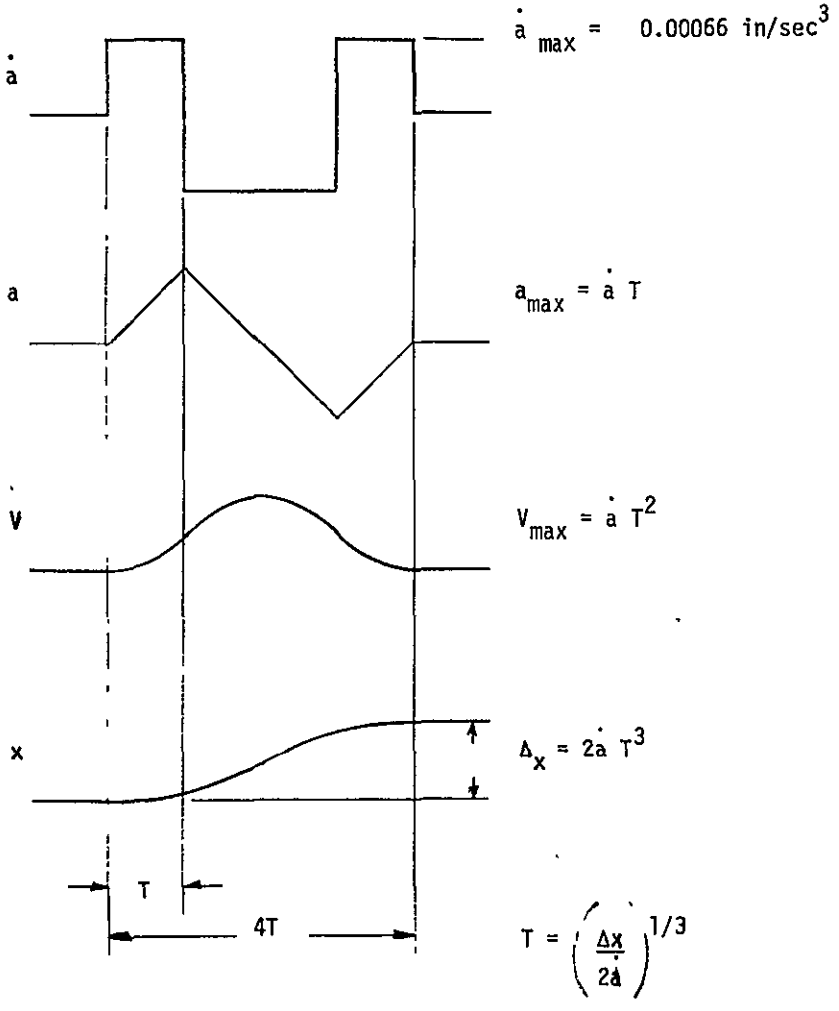

FIGURE 3.7-2

TIME REQUIRED TO MOVE SENSOR HEAD BETWEEN SEPARATED STARS

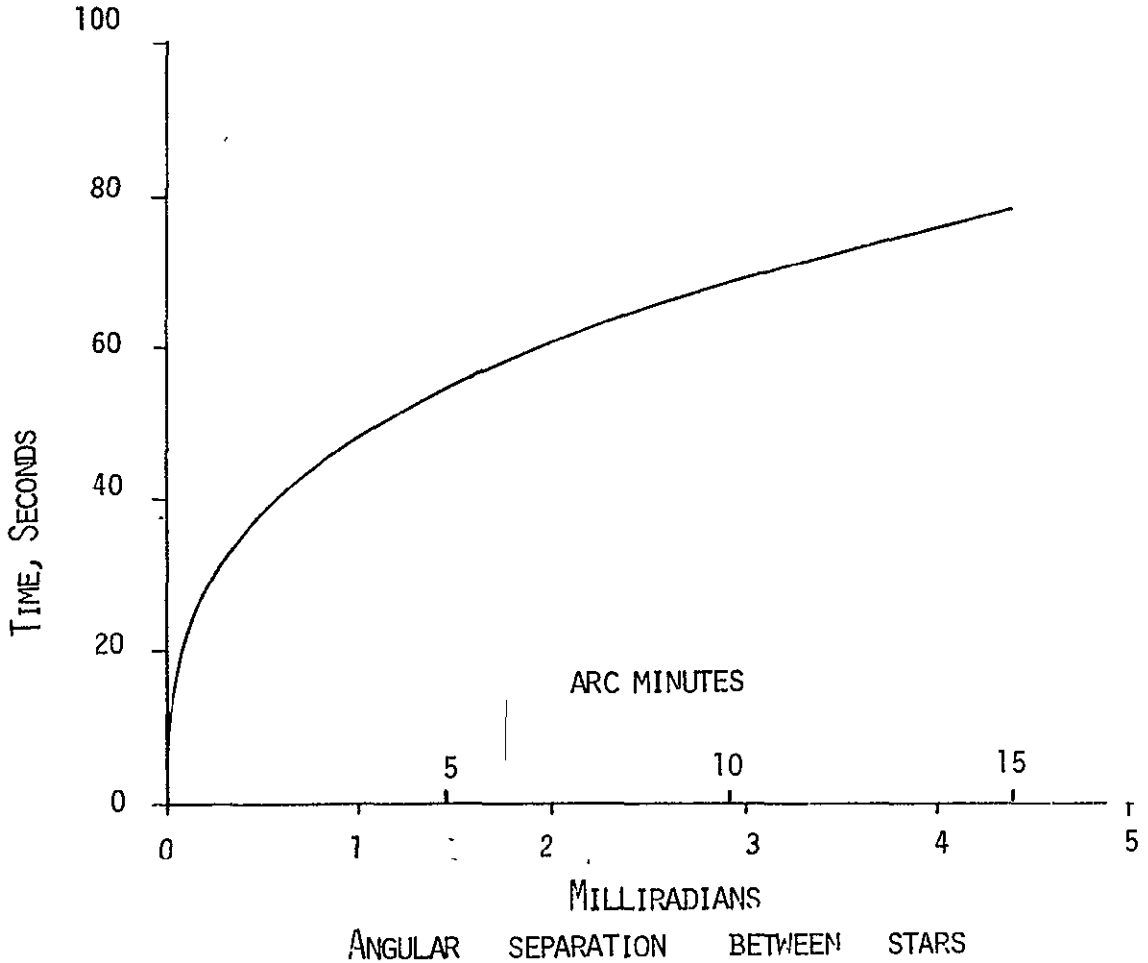

In the sensor head drive mechanism, the primary sources of disturbance are changes in the friction level, quantization ripple*, gearing error in the sector drive and pinion, and tachometer switching. Use of a ball screw in the radial drive is avoided because of the disturbance from ball re-entry that would accompany it. Instead, a rolling nut is used.

Line-of-sight disturbances calculated for these disturbances are given in Table 3.7-1 for both body disturbances and elastic disturbances. The calculations indicate that the simple rigid-body disturbances are the most severe, and that in all cases, the peak disturbances are within tolerable limits.

The most severe disturbance from the optical micrometer is flyback during solar system observation. The flyback occurs in 0.2 second with a limited-acceleration profile. The micrometer disturbances shown in this table are within tolerable limits. Again, the body disturbance is most significant.

TABLE 3.7-1

LINE-OF-SIGHT MOTIONS FROM
FINE GUIDANCE SENSOR MECHANISMS

	PEAK LOS MOTIONS, MICRORADIANS		
	BODY POINTING	TRANSIENT ELASTIC	RESONANT ELASTIC
SENSOR HEAD MECHANISM			
Motion Profile	0.005	0	0
Friction Torque	0.0035	0.00001	0
Quantization Ripple	0.00001	0	0
Gearing Error	0.002	0.00004	0
Tachometer Switching Ripple	0.0005	0	0.0003
OPTICAL MICROMETER	0.004	0	0

3.8 Off-Shelf Components

Table 3.8-1 is a list of the off-the-shelf components used in the design.

* The ripple introduced by a digital feedback comparator in the servo.

TABLE 3.8-1

FINE GUIDANCE SENSOR COMPONENTS

		QTY.	WT. EA. LB.
Image Dissector	ITT 4011-RP	1	0.34
Reflection Assembly	ITT Type F4534	1	3.63
ρ, θ Drive Motors	Inland T-1342	2	0.62
ρ, θ Drive Tachometers	Inland TG-1312	2	0.31
ρ, θ Resolvers	Clifton CR 64 1X, 1.838" OD	2	0.25
Micrometer Drive Motors	Aeroflex TQ 18W-23	2	0.25
Micrometer Resolvers	Clifton CR 64 1X, 1.838" OD	2	0.25
Filter Drive Motor	Clifton MSL-8-A-1 Stepper	1	0.11
Shutter Motor	Aeroflex TQ 18W-23	1	0.25
Shutter Brake	Magtrol FB 59	2	0.44
Launch Lock Motors	Aeroflex TQ 18W-23	2	0.25
Launch Lock Brakes	Magtrol FB 59	2	0.44
ρ Drive Slides	Rotolin #ML 62501000-2 (5/8" Shaft)	3	

3.9 Power Profile

Figure 3.9-1 gives the power profile for the pointing and control system of the OTA. It is based upon power for a single fine guidance sensor as follows:

Electronics	50 Watts
Power for Servos	24 Watts
Image Dissector	10 Watts
Thermal Control	5 Watts

The power conditioner unit is assumed to be 75% efficient. Taking into account the power dissipated by the power regulation, the total power is 118 watts for one fine guidance sensor (thermal control power is unregulated).

During operation of the sensors, the power level is virtually constant. If astrometry is performed with the third sensor, additional power is consumed, coming from the SI power allotment.

FIGURE 3.9-1

POINTING AND CONTROL POWER PROFILE

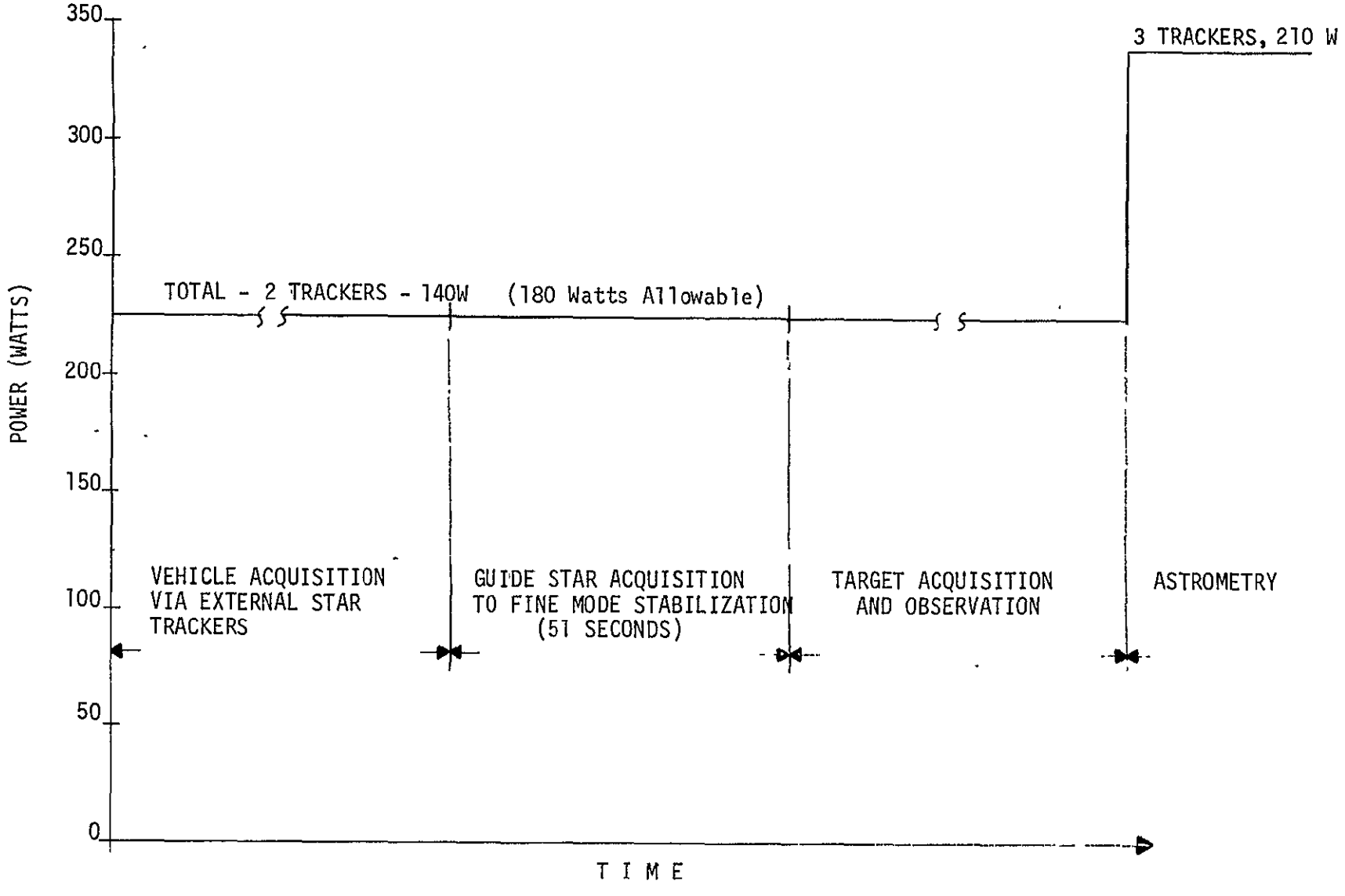

4.0 ASTROMETRIC USES OF THE FINE GUIDANCE SENSOR

4.1 General

The fundamental use of the fine guidance sensor for astrometry is star position measurement using the lock-on capabilities of the sensor. While two sensors maintain the line-of-sight stable, the third sensor can measure the relative positions of several stars in its field. The star positions are known approximately ($\pm$ 2 arcsec) beforehand. The sensor head is positioned behind the first star image, the image is centered on a grating intersection using the optical micrometer, and the optical micrometer angle is read out to indicate the position of the undeflected star image relative to the grating intersections. This basic technique was outlined in Table 2.0-1.

Another technique for measuring relative star positions uses the optical micrometer to scan the star image across the grating. The photon counts are recorded at regular intervals as the star is scanned. Subsequent ground analysis of the profiles determines the star centers. This method requires more time and data storage, but can measure star positions accurately even with other stars very close by. (See Section 4.3 for more detail.)

The fine guidance sensor can be used for double star detection during the course of normal star position measurement. Detection of double stars not resolvable from the ground but resolvable by the ST can be made by means of a coarse scan of the known star across the grating using the optical micrometer.

On-board processing of the scanned profile can be used for the detection, whereupon a fine scan of each distinct star will provide data for accurate measurement of their separation.

In summary, the astrometric uses of the fine guidance sensor are:

Star Position Measurement by Lock-On
Star Position Measurement by Scanning
Double Star Detection
Double Star Separation Measurement

DENSELY POPULATED AREAS

The fine guidance sensor generally might make astrometric measurements in the manner of operation used for fine stabilization. The sensor locks onto a particular star with the telescope stabilized via the other two fine guidance sensors. The optical micrometer angle then indicates the position of the star image relative to the coordinates of the grating.

In densely populated areas of the sky, however, another star close to one of the stars being measured can bias the measurement of that star alone, resulting in an error in the star separation measurements. If the position of an M_V 17 star were being measured, for example, an M_V 22 star image within

one of the four grating facets admitting light into the image dissector would result in a 1% offset in the energy balance of the null measurement. The stars have an effective image width of 0.42 microradians, and so the 1% energy imbalance would result in a 0.0042 microradian (0.0009 arcsecond) measurement error. This would probably be tolerable, but stars of M_V 21 or brighter would result in an unacceptable offset.

Figure 4.1-1 shows the probability of finding a star of a given magnitude or brighter within a small field width in the fine guidance sensor at the Galactic equator, the region of the sky with maximum star population density. The curve from the figure that applies is the 20 microradian aperture curve, since this is the equivalent aperture width of four grating facets together.

Figure 4.1-1 indicates that, at the Galactic equator, there is about a 30% probability of finding an M_V 21 or brighter star within the 20 micrometer-wide aperture. Thus, in this part of the sky, offset errors resulting from close stars would be very common.

Figure 2.0-2 indicates that for the sky as a whole, M_V 21 stars are about 3 times less common than at the Galactic equator. The probability of having a significant offset error when measuring an M_V 17 star would, on the average, be about 7%. Even in the average case, therefore, the scanning technique would be desirable to avoid the possible bias effects of another nearby star.

4.2 Calibration

The fine guidance sensor can be self-calibrating by the use of certain calibration routines, with the exception of the grating calibration for astrometry, which must be performed on the ground. This calibration is performed on special equipment that calibrates the grating in the same manner in which it is used. Since all gratings are made from a single set of masters, it is conceivable that the grating could be calibrated from a replica on the ground even after the ST is launched. The calibration is described in more detail in Section 4.5.

The photocathode sensitivity variations between the four fields can be calibrated by successively imaging a star in the four adjacent grating facets and measuring the relative outputs of the image dissector. This calibration is not critical, however. Offset errors in measurements using the lock-on technique will be common to all stars measured, and thus will not reside in the final relative position measurements. The scanning technique is inherently insensitive to differences in the photocathode sensitivity.

The image dissector aperture response is expected to be sufficiently uniform, but it can be checked by performing an aperture scan of a bright star image.

Centering of the image dissector aperture on the grating facet image is accomplished by a special calibration routine described in Figure 3.4-2.

The scale constant of the optical micrometer will be a function of star color, because of the variation of the index of refraction. The scale is, therefore, calibrated for each star measurement. The procedure is simply to use the micrometer to lock on with the star at two adjacent grating intersections. The calibration is obtained from the measured micrometer deflection and the known separation between the grating intersections.

FIGURE 4.1-1

MAXIMUM STAR DENSITY

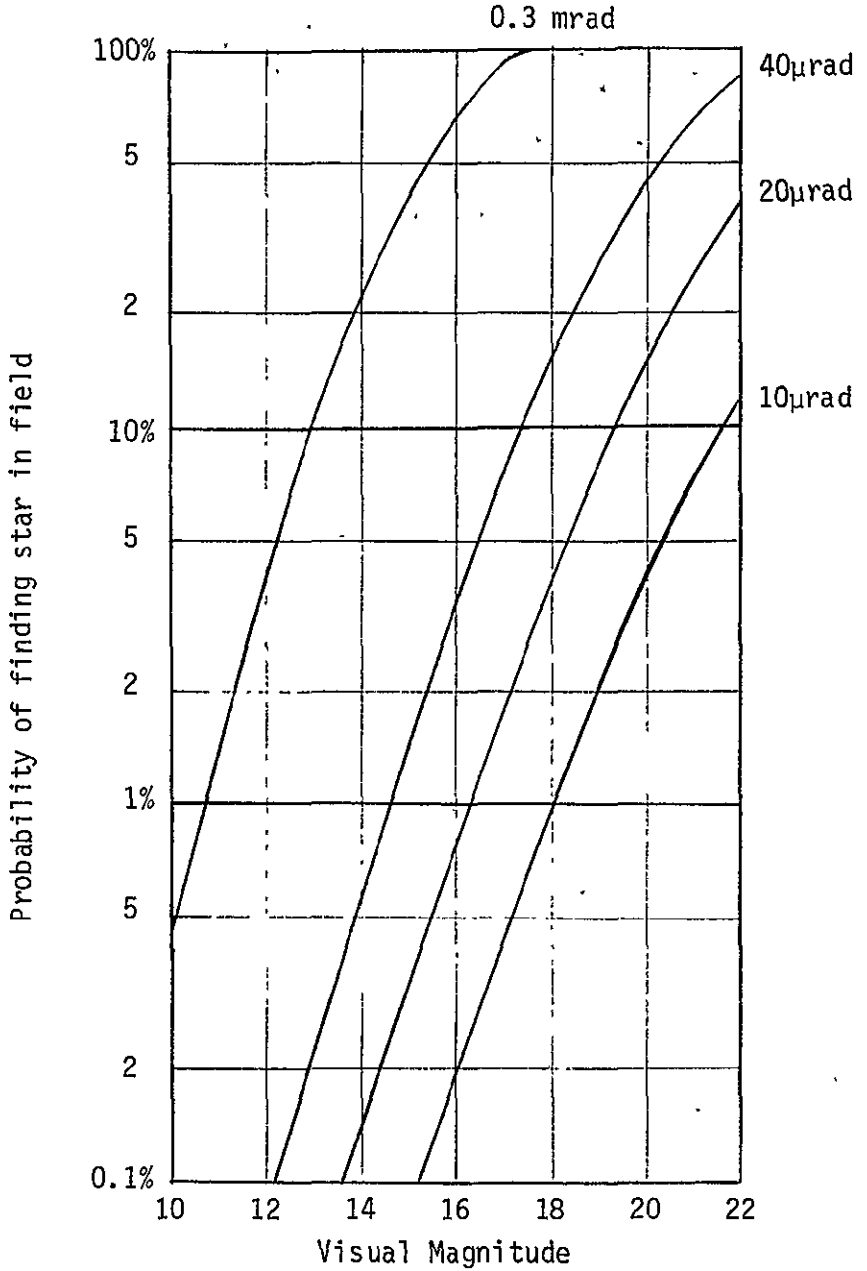

Probability of Finding a Star in fields of various sizes at Galactic Equator (Based upon Poisson distribution)

10μrad -- Grating facet width

20μrad -- Image dissector aperture width

0.3mrad -- Acquisition field of Sensor Head.

Table 4.2-1 summarizes the calibrations for astrometry.

TABLE 4.2-1

CALIBRATION FOR ASTROMETRY

FEATURE TO BE CALIBRATED	MEANS OF CALIBRATION
Grating	Calibration Equipment on Ground
Photocathode Uniformity	Image Star Successively in Four Adjacent Facets
Image Dissector Aperture Uniformity	Aperture Scan of Single Star Image
Aperture Centering	Aperture Nutation
Optical Micrometer Color	Measurement at Adjacent Grating Peaks

4.3 Star Center Determination By Scanning

In making astrometric measurements with the fine guidance sensor by the scanning technique, the star will be scanned across a grating ridge via the optical micrometer, and the edge spread function will be recorded through each of the four optical channels. The edge spread function will then be processed in order to determine the center of the star. In order to determine what integration times and scan rates are required, it is necessary to consider a particular processing technique for analysis.

If the waveform of a signal is known, its position can be determined near-optimally if the signal is first filtered by means of a matched filter having the same waveform as the signal itself. Conceptually, then, the first steps in determining the position of a star will be to differentiate the edge spread function to get the line spread function, and then convolve the resulting image pulse with a filter function that has a similar shape. In practice, the differentiation will be applied to the filter function before convolution.

Convolution of the edge-spread function with the differentiated filter function will give a pulse whose ordinate is a number of photon counts. The center of the star can then be found by finding the mean abcissa value corresponding to the predetermined level of photon counts at a location on either side of the peak of the function.

Figure 4.3-1 illustrates the general process of star center determination by scanning. The following analysis was performed in order to estimate what the noise errors of this process would be.

FIGURE 4.3-1

STAR CENTER DETERMINATION

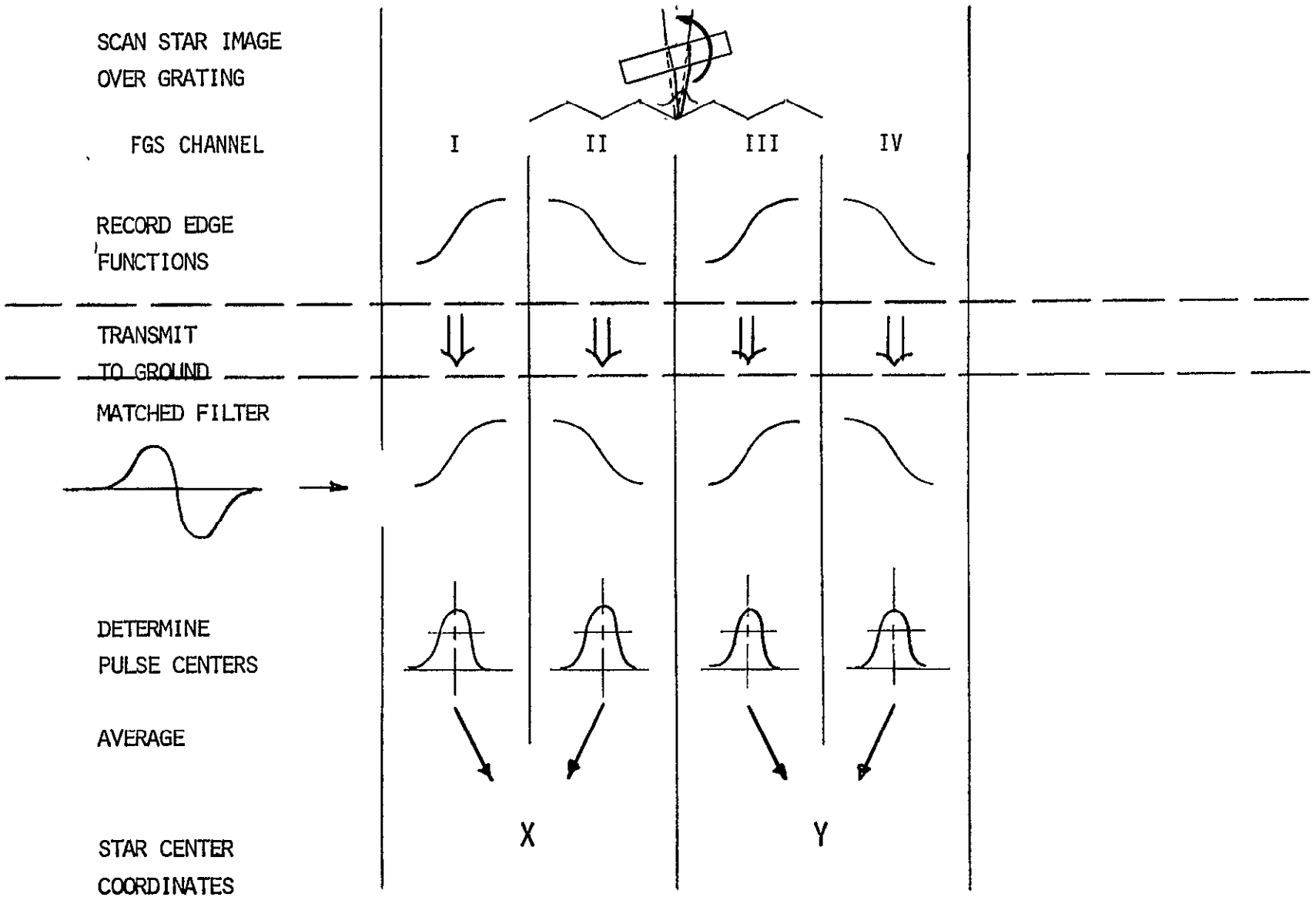

Suppose that in recording the image, the optical micrometer is scanned along at such a rate that N' photons are recorded per micrometer distance in the focal plane. The effect of the grating will be that the actual photons recorded will have the function N' y(x), in which y(x) is the edge spread function as shown in Figure 4.3-2. Differentiation of the edge spread function will give the line-spread function, y'(x). Convolution of the line-spread function with a filter function of similar form will give a pulse whose ordinate is a number of photon counts, as shown in Figure 4.3-2. The center of the star can then be found by finding the mean abcissa value corresponding to a predetermined level of photon counts at a location on either side of the peak of the function.

The convolved function is

$$N(X) = N' \int_{-\infty}^{\infty} f(x - X)\, y'(x)\, dx$$

This function can also be determined by convolving f'(x), the derivative of f(x), directly with the edge spread function, y(x):

$$N(X) = N' \int_{-\infty}^{\infty} f'(x - X)\, y(x)\, dx$$

This latter convolution is what most likely would be used in processing.

In order to determine the accuracy with which the star center can be determined, it is necessary to calculate the uncertainty in the photon count function N(X) resulting from the photon noise in the signal. In the second convolution integral above, the rms uncertainty in the quantity N'y(x) dx is $\sqrt{N'y(x)\, dx}$, and so the rss error in N(X) is

$$\Delta N(X) = \sqrt{N' \int_{-\infty}^{\infty} f'^2(x - X)\, y(x)\, dx}$$

The error in finding the center of the pulse is determined by the photon count uncertainty on both sides of the pulse:

$$\Delta X = 1/2 \; \frac{\sqrt{\Delta N^2(X-) + \Delta N^2(X+)}}{dN(X) / dX}$$

Since the errors from both sides of the convolved pulse contribute to the error in star center determination, the total photon count uncertainty is

$$\Delta N(X+,-) = \sqrt{N' \int_{-\infty}^{\infty} f'^2(x)\, dx}$$

because $y(x + X) + y(x - X) = 1$

The error in star position determination is then,

$$\Delta X = 1/2 \; \frac{\Delta N(X+,-)}{dN(X) / dX}$$

in which dN(X) is the slope of the convolved function at the point used in determining the star center. The error is minimized if the point of maximum slope is used.

Figure 4.3-2 - Processing Functions

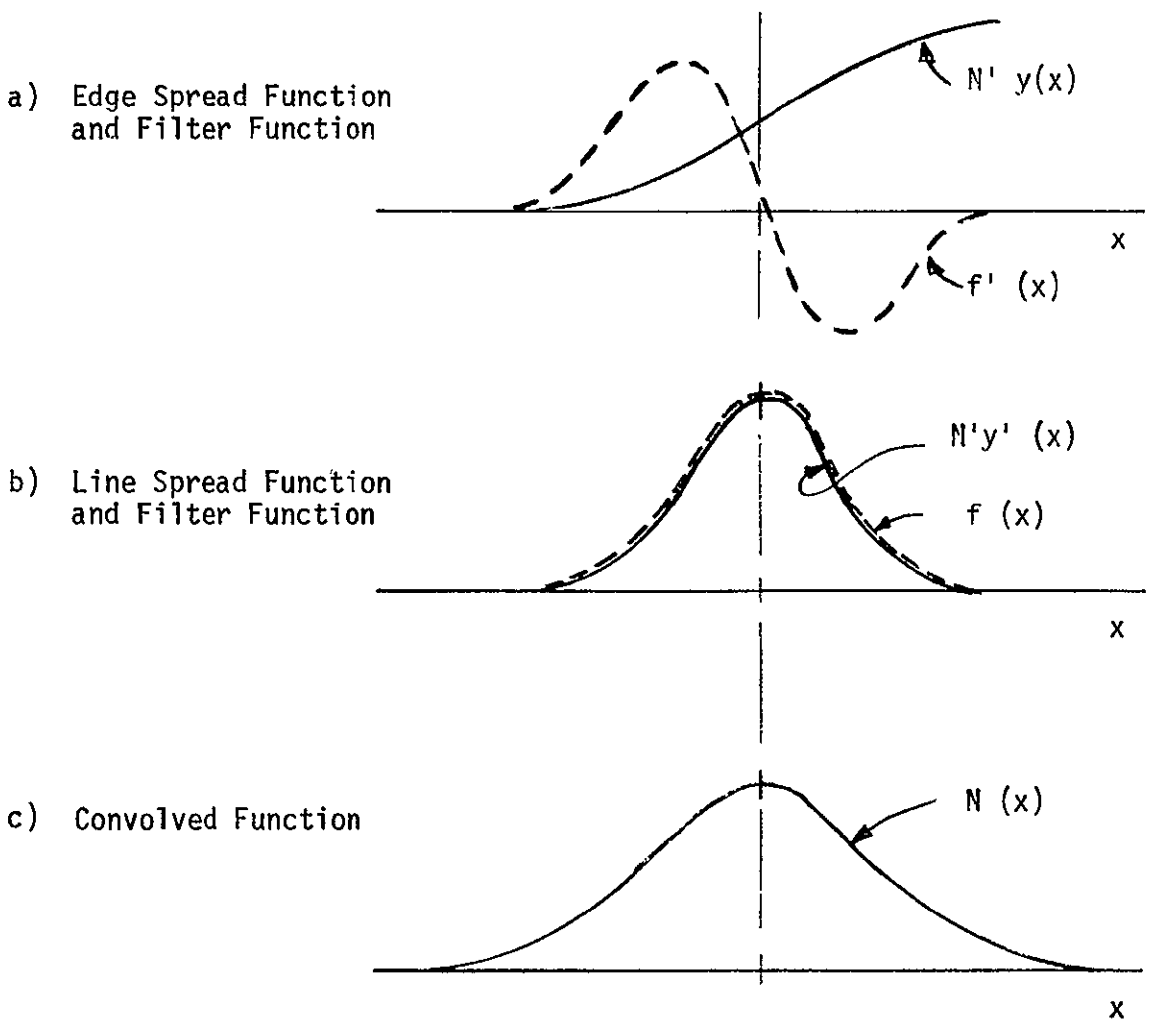

For the purpose of analysis, the line spread function can be approximated by a Gaussian distribution. Figure 4.3-3 shows the line spread function corresponding to the worst-case image with the optical micrometer in its fully-deflected position. Super-imposed upon the line spread function is a Gaussian function whose rms value is 10 micrometers.

For the analysis, it has been assumed that

$$y'(x) = \frac{1}{a\sqrt{2\pi}} \quad e^{-x^2/2a^2}$$

for which the integrated value is 1.0, and that

$$f(x) = a\, e^{-x^2/2a^2}$$

$$f'(x) = -(x/a)\, e^{-x^2/2a^2}$$

The convolved pulse function is

$$N(X) = (N'a/\sqrt{2})\ e^{-X^2/4a^2}$$

This has a slope

$$dN(X)/dX = -(N'/\sqrt{2})(X/2a)\ e^{-x^2/4a^2}$$

which has a maximum value at $X/2a = 1/\sqrt{2}$;

$$dN(X)/dX\ (max) = -0.303\ N'$$

The rms image position uncertainty works out to be:

$$\Delta X = \sqrt{2.41\ a/N'}$$

for a = 10 micrometers,

$$\Delta X = \sqrt{24\ \text{micrometers}/N'}$$

The quantity N' is the photon arrival rate, $\dot{N}$, divided by the scan velocity, v. For a given star measurement uncertainty,

$$v = 0.415\ \Delta X^2\ \dot{N}/a$$

so that for a = 10 micrometers, ΔX = 0.01 microradian (0.576 micrometer at f/24), and $\dot{N}$ = 130 photoelectrons/second for a M_V 17 star (c.f. $\dot{N}$ = 5100/sec for M_V 13), the scan velocity v is 1.79 micrometer/second (0.031 microrad/sec object angle).

COARSE AND FINE SCANNING

Two different scans may be desirable: a coarse scan over one facet-width distance to identify distinct stars, and a fine scan over the image width of one star to determine its center precisely. The output from the coarse scan would be processed on-board so that individual stars thus identified could be fine-scanned. Without the coarse scan, the sensor will lock on to the predominant star, and then the fine scan will be centered at the lock-on location. The second star will not be detected. Figure 4.3-4 illustrates these scans.

FIGURE 4.3-3

LINE SPREAD FUNCTION & GAUSSIAN FILTER FUNCTION FOR STAR CENTER DETERMINATION

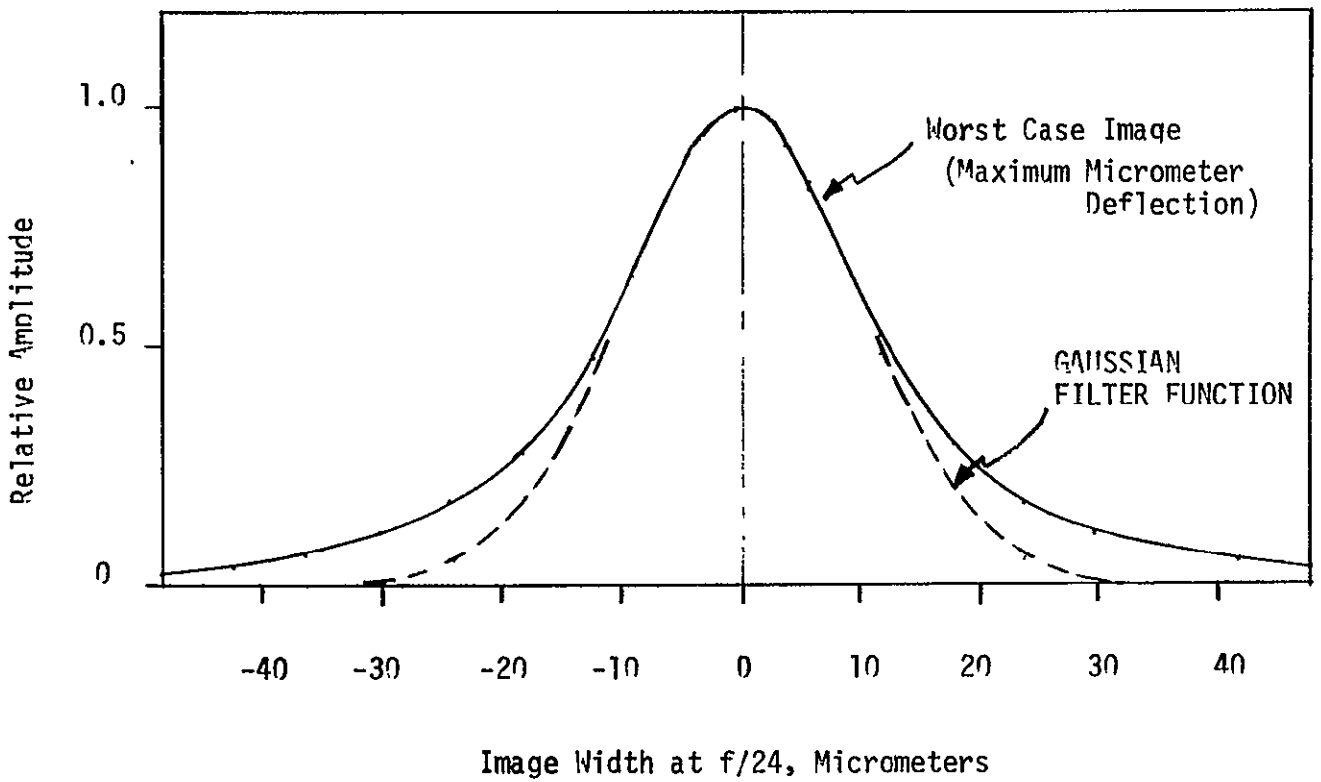

FIGURE 4.3-4

COARSE AND FINE SCANNING WITH THE OPTICAL MICROMETER

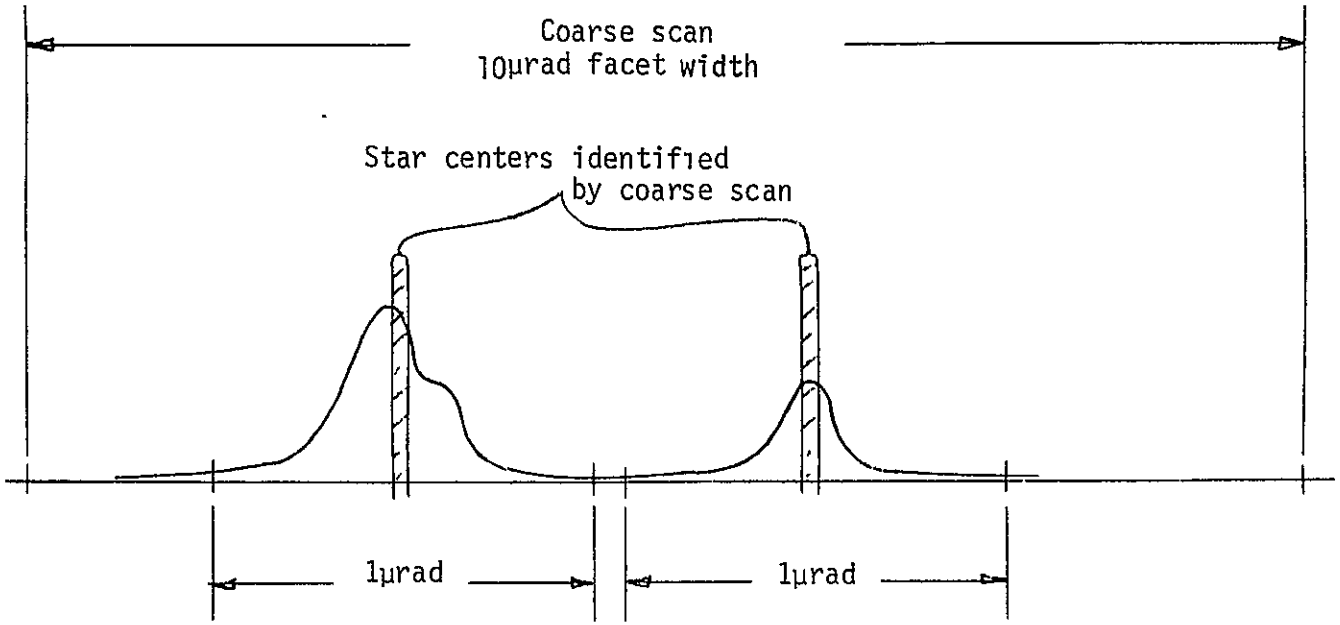

Fine scan for star characterization

The scan motion is generated by both plates of the optical micrometer so that the actual image motion is diagonal across the grating facet. The scan signals for the orthogonal directions are then recorded simultaneously.

Table 4.3-1 gives the features of each scan for measuring M_V 17 stars.

The calculations were made using:

$$a = 10 \text{ Micrometers (RMS Image Width)}$$

$$\dot{N} = 130 \text{ Photoelectrons/Second}$$

TABLE 4.3-1

OPTICAL MICROMETER SCANS FOR ASTROMETRY

(Measuring M_V 17 Stars)

SCAN	FINE	COARSE
RMS CENTER UNCERTAINTY	0.01 μRAD	0.1 μRAD
SCAN VELOCITY	0.031 μRAD/SEC	3.1 μRAD/SEC
SCAN LENGTH	1 μRAD	10 μRAD
SCAN TIME	32 SECONDS	6.4 SECONDS

4.4 Sequence of Events for Astrometry

Table 4.4-1 shows the sequence of events for an astrometric measurement of one star, assuming that all measurement modes are used.

First, the lock-on to the star is achieved. The sensor head is positioned behind the star image (as accurately as the star position is known). Fine lock-on to a grating intersection is accomplished using the optical micrometer in a closed-loop mode. The magnitude is verified. The routine for the calibration of the image dissector deflection (Section 2.4) is performed and the image dissector aperture is then centered on the grating facets surrounding the grating intersection of interest. The star center is identified from the optical micrometer position. The optical micrometer scale calibration is then performed which involves lock-on at an adjacent grating intersection and recording the micrometer position.

The coarse scan involves resetting the image dissector aperture, presetting the optical micrometer, scanning and recording photon counts at fixed intervals and on-board processing to identify and determine the centers of distinct stars.

The fine scan involves presetting the optical micrometer and scanning the image with the optical micrometer while recording the photon counts. This data is stored for transmission to ground for processing.

TABLE 4.4-1

SEQUENCE OF EVENTS FOR ASTROMETRY

LOCK-ON AND CALIBRATION

- Position Head
- Fine Lock-on With Optical Micrometer
- Verify Magnitude
- Calibrate Image Dissector Deflection
- Center Image Dissector Deflection
- Center Image Dissector Aperture on Grating Intersection
- Identify Star Center
- Reposition Aperture Position for Micrometer Scale Calibration
- Lock-on With Optical Micrometer at Adjacent Position
- Identify Star Center

STAR MEASUREMENT

Coarse Scan

- Center Image Dissector on Grating Facets
- Set Optical Micrometer
- Scan Optical Micrometer
- Record Photon Counts
- Convolution with Filter and Star Center Determination
- Convert to Half Magnitudes and Location
- Identify Positions for Measurement

Fine Scan

- Center Image Dissector on Grating Facets
- Set Optical Micrometer
- Scan Optical Micrometer
- Record Photon Counts

4.5 Astrometry Errors

Besides the measurement uncertainty associated with the photon statistics, a number of error sources within the fine guidance sensor limit the accuracy of relative measurements of star positions. The error sources and their estimated values are shown in Table 4.5-1.

The most fundamental source is the accuracy with which the grating intersections are known. The grating is calibrated on the ground, and the accuracy of this calibration determines the measurement accuracy of the sensor. The calibration method planned would involve measurement of the grating intersection positions with a technique which mimics the actual use of the gratings. A small, movable optical system would focus an astigmatic point image upon the grating. Radial position, tangential position, and tip/tilt of the optical system would be measured, respectively, with a laser interferometer, a precision indexing table, and autocollimators. The optical system would be centered at each intersection by servo control from a quad cell behind the grating. Position then would be measured. Available laser interferometers can measure to 1×10^{-6} inch, while precision indexing tables are accurate to 0.1 arcsecond. Those numbers are consistent with grating calibration to 0.005 μrad object angle.

On board, the grating will change its size slightly with changes in temperature. The only size change that affects the measurement is that which occurs during the measurement since determination of absolute scale at the time of measurement will be made from the number of stars measured. A temperature change of about 0.1°C can be expected in a 10 minute interval.

The focal plane housing relates the three fine guidance sensors to each other. Since two of the sensors are used to stabilize the line-of-sight while the third is measuring star positions, growth of the housing will introduce a line-of-sight change at the sensor being used for the measurements. Similarly, guidance errors which don't have a zero average value will affect the measurements. These are the sensor-related errors as they apply to fine stabilization.

The micrometer resolver error and the micrometer quantization result in direct measurement errors. Any tip of the micrometer mount produces a line-of-sight deviation not recorded on the micrometer resolver.

Gradients in the sensitivity of both the photocathode and the electron multiplier aperture across its width can be expected. These gradients arise from the non-uniformity of response, as represented in Table 3.3-2. The non-uniformity tends to be a smooth, parabolic function over the faceplate and aperture, respectively. Of the two, the gradient across the aperture width will predominate.

The RSS value of these errors, referred to line-of-sight error, is 0.01 microradian (0.002 arcsecond). This should be considered a high probability value (two- or three-sigma), since the individual errors are calculated on the basis of error limits rather than average errors.

TABLE 4.5-1

ASTROMETER ERRORS

ERROR SOURCE		ERROR, μRAD
Grating Intersection Calibration		0.005
Grating Thermal Growth - 0.1°C in 10 Min.		0.0003
Focal Plane Housing Growth - 0.5°C in 10 Min.		0.002
Guidance Error During Measurement (Bandwidth-Independent Errors)		0.0053
Micrometer Resolver Error (15 Arcseconds)		0.0028
Micrometer Quantization Error (13 Bits)		0.0014
Micrometer Mount Tip (15 Arcseconds)		0.0028
Electron Multiplier Sensitivity Variation Across Aperture		0.0007
	RSS	0.010 (0.002 Arcsec)

4.6 Double Star Measurements

An estimation of the ability of the fine guidance sensor to measure the separation between close double stars was based upon the position uncertainty for a single star measured using the scan technique. How the estimation was made is illustrated in Figure 4.6-1.

For a single star, the time required to scan over one microradian is a function of the photo electron rate, $\dot{N}$, and the desired position uncertainty, σ_θ.

When a brighter star is nearby, within one grating facet width but distinctly separated from the dim star whose position is being measured, the scan time must be extended to overcome the photon noise introduced by the light from the bright star. The intensity of the bright star is I_b, while the intensity of the dim star being measured is I_d. $F(\Delta\theta)$ is the value of the line-spread function of the bright star at the center of the dim star. This determines the residual light from the bright star in an adjacent facet of the grating just as the dim star is scanning out of one facet into the adjacent facet.

When the two stars are not distinctly separated, the resolution limitations of the telescope come into play. The time of the measurement is extended by the reciprocal of the value of the telescope MTF at the frequency corresponding to the star separation distance, $\Delta\theta$.

FIGURE 4.6-1

BASIS OF DOUBLE STAR MEASUREMENT CALCULATIONS

DIM STAR = $M_V 17$

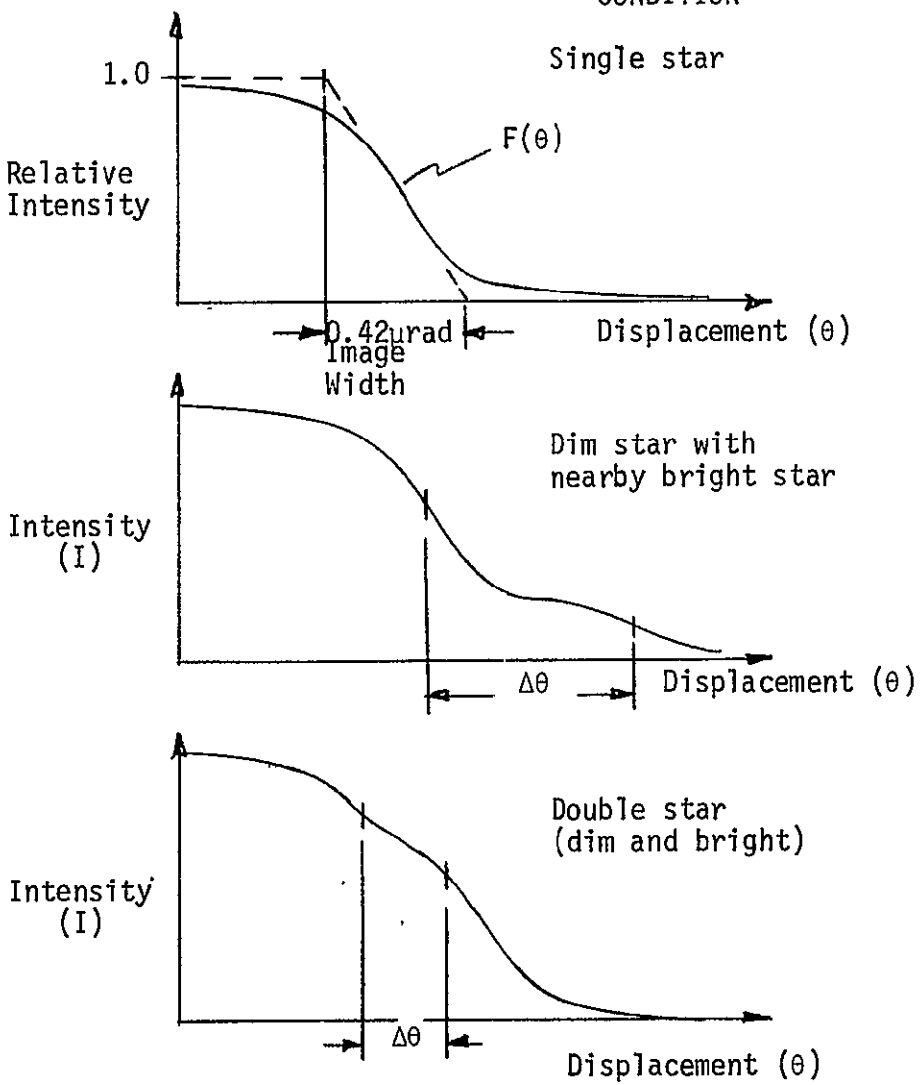

Further limitations to the capability to measure double stars will result from the lack of symmetry of the line spread function. Figure 4.6-2 shows the line spread functions computed for the combined OTA and optical micrometer with the image undeflected by the optical micrometer and with the image deflected by the maximum amount. The OTA has 0.055 waves RMS random wavefront error (at 0.6 micrometer) with a correlation distance of 30% of telescope aperture, plus the predicted OTA defocus. The randomness of the wavefront error is the cause of the irregularity of the higher order diffraction bands of the function. To some extent, these can be taken into account in the ground processing. As the peak intensity of the line spread function of the dim star goes below the intensity of the line-spread function of the bright star, measurement of the separation will become rapidly more difficult (equal amplitude condition, figure 4.6-2).

Figure 4.6-3 shows the calculated uncertainty in measurement of the separation between two stars not distinctly separated, when the dimmer of the two stars is of visual magnitude 17 and the scan time is 32 seconds. The measurement uncertainty is shown as a function of the star separation and the visual magnitude of the bright star.

The equal amplitude boundary shown is the locus representing the equal-amplitude condition for the dim star as defined in Figure 4.6-2. It represents the conditions at which the measurement becomes more and more difficult because of the irregular diffraction bands in the image that will tend to be confused with true double stars. For conditions represented by points below this boundary, the measurement capability given by the chart readily can be obtained, but for conditions represented by points above the boundary, more and more sophistication in the data processing, involving careful calibration of the line spread functions, accounting for star color effects, etc., will be necessary in order that the measurements approach the accuracy given by the chart.

4.7 Time Required for Astrometry

The time required for astrometry varies considerably with a number of factors. The time that it takes to move the sensor head depends upon the actual disturbance rejection characteristics of the body pointing control system. It probably will take up to two minutes to move the sensor head the full length of the grating. Time on the order of 1/2 minute is probably average, as was discussed in Section 3.5.

The time to perform the measurement depends upon the star brightness and the measuring options being used, but the measurement time generally will be one minute or less. The average total time will be on the order of 1 - 2 minutes per star, being the sum of the sensor head transit time and the star measurement time.

FIGURE 4.6-2

LINE SPREAD FUNCTION OF IMAGE AT GRATING

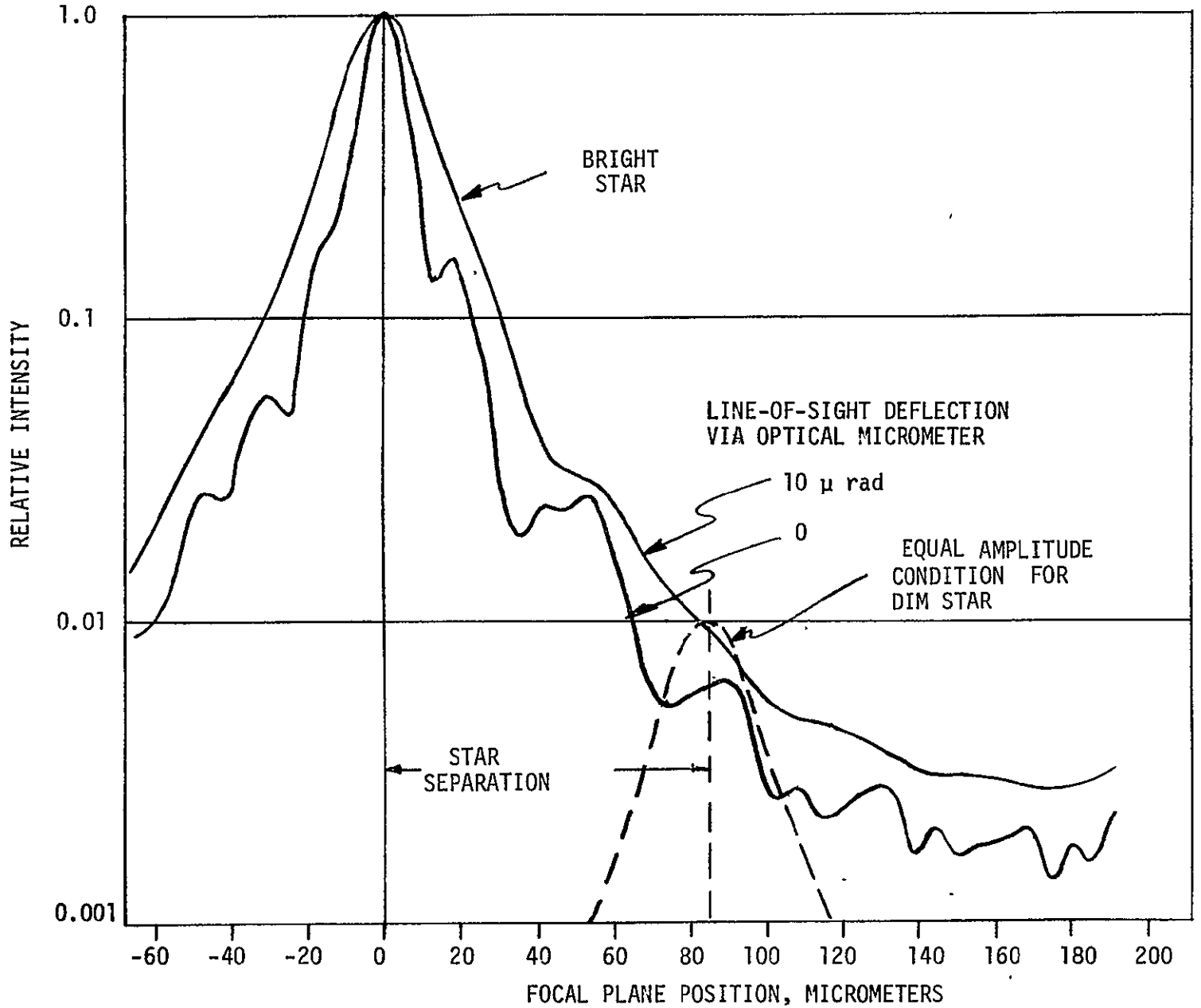

FIGURE 4.6-3

DOUBLE STAR MEASUREMENT UNCERTAINTY

MEASUREMENT OF A M_V 17 STAR CLOSE TO A BRIGHTER STAR

32 SECONDS TO SCAN 1μRAD

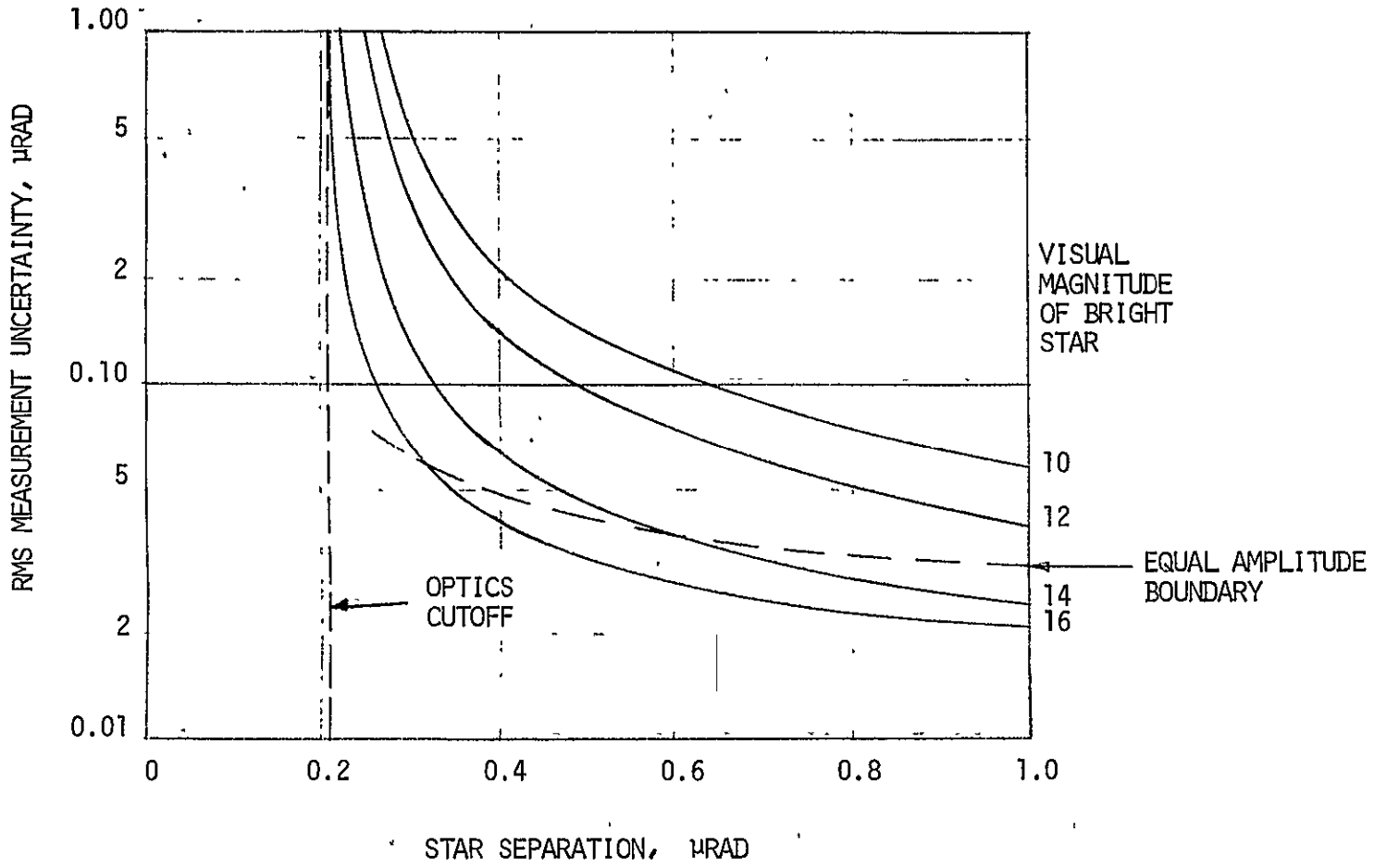

4.8 Fine Guidance Sensor Command and Data Lists

The command, output, and data lists for the Fine Guidance Sensors are shown in Tables 4.8-1, 4.8-2, and 4.8-3, respectively. These lists have been taken from Volume IIB, Optical Telescope Assembly, in which they are explained in detail with regard to fine guidance. The additions to the FGS which enable it to perform astrometry are reflected in the FGS command, output, and data lists as indicated in the tables.

As an aid to understanding how the commands and data are used in the performance of astrometry, Table 4.8-4 has been generated. This table integrates the commands, outputs, and data of Tables 4.8-1, 4.8-2, and 4.8-3 with the events for astrometry listed in Table 4.4-1. The table distinguishes between ground activity, activity within the on-board computer, commands to the FGS, activity within the FGS, and FGS output and data.

TABLE 4.8-1
FINE GUIDANCE SENSOR COMMAND LIST (EACH SENSOR)

COMMANDS FROM SSM			FUNCTIONAL RESULT							COMMAND RANGE QUANTIZATION	
COMMAND	TYPE		INITIALIZE	FGS POSITION SENSOR HEAD	PHASE OF OPERATION					RANGE	LSB(QUANTIZAT
	DISCRETE	MULTIBIT BITS			ACQUIRE	COARSE TRACK	FINE TRACK	SOLAR TRACK	** DVA		
*Sensor Select		2									
Open Shutter	x		x								
Close Shutter	x										
Activate Launch Locks	x										
Deactivate Launch Locks	x		x								
Micrometer Calibration	x										
Photocathode Calibration	x										
Deflection Calibration	x										
Deflection Reset	x										
Acquire & Lock-on Command	x				x	x	x				
Select Mode (Pitch/Yaw, Roll, Focus, Astrometry)		3	x								
Set Focus Current		8	x								
Set Anode Voltage		8	x								
Select Pwr. Configuration		4	x								
Select Stellar Magnitude		7	x								
Guide Star Polar Coord Position ρ		21	x	x				10/sec Update Rate		5 μrad	0.002
Guide Star Polar Coord Position θ		24	x	x				10/sec Update Rate		360° 28.3μrad LOS)	0.4 μ (0.0018 LOS)
Guide Star Polar Coord Rate $\dot{\rho}$		11						10/sec Update Rate		3 μrad/sec	0.0014 μrad/
Guide Star Polar Coord Rate $\dot{\theta}$		11						10/sec Update Rate		667μrad/sec 3 urad/sec LOS	0.3 μr/s 0.001 μrad
Set Exposure Time (Focus, Astrometry)		3	x								
Select Filter (Astro.)		3	x								
Duration of Phase(Max.Sec)			2	80	15	15	Continuous				

60

The sensor select is to select one of the three sensors and is therefore common to all three

** Update guide star coordinates as required

TABLE 4.8-2
GUIDANCE OUTPUTS (EACH SENSOR)

OUTPUTS FROM FGS TO SSM			FUNCTIONAL MODE					OUTPUT RANGE AND QUANTIZATION	
	DISCRETE	MULTIBIT BITS	GUIDE STAR ACQUIRED	COARSE TRACK	FINE TRACK	SOLAR TRACK	OBSERVE	RANGE	LSB
Guide Star Acquired	x		x						
Micrometer Flyback	x					x			
Fine Lock-on Verification					x				
Radial Coarse Error ($\Delta\rho$)		10		25/sec *				$\pm$0.15mrad	0.29µrad
Tangential Coarse Error ($\Delta\Theta$)		10						+0.33 rad ($\mp$0.001485 rad LOS)	60µrad (0.27µrad LOS)
Radial Fine Error ($\Delta\rho$)		11			100/sec*	100/sec*	100/sec*	$\pm$1.64µrad	0.0016µrad
Tangential Fine Error ($\Delta\Theta$)		11			100/sec*	100/sec*	100/sec*	+0.365mrad ($\mp$0.001643µrad LOS)	0.36 µrad (0.00162µrad LOS)
Duration of Phase			--	15 sec max	Continuous				

* Output Sample Rates

TABLE 4.8-3

FINE GUIDANCE SENSOR DATA LIST (EACH SENSOR)

DATA	DISCRETE	MULTIBIT BITS	ANALOG
Filter Wheel Position		3	
Shutter Open	x		
Shutter Closed	x		
Sensor Head Position - Radial		10	
Sensor Head Position - Tangential		10	
Micrometer Position - Radial		13	
Micrometer Position - Tangential	13		
Voltage 1			x
Voltage 2			x
Voltage 3			x
Voltage 4			x
Voltage 5			x
Voltage 6			x
Voltage 7			x
Current 1			x
** Surface 1 Defocus		14	
** Surface 2 Defocus		14	
* Photon Count		14	
Deflection Error		12	
Deflection Constant		18	

* Astrometer Output Data and Photocathode Calibration

** Focus Sensor Output Data

TABLE 4.8-4 USE OF FGS COMMANDS AND DATA FOR ASTROMETRY

GROUND DETERMINATION	ON-BOARD COMPUTER	COMMAND (Table 4 8-1)	FGS ACTIVITY	FGS OUTPUT DATA (Table 4.8-2)	FGS DATA (Table 4.8-3)
Star location and magnitude, filter, command sequence, exposure times	Transmit commands to FGS	Guide star coordinates Filter command	Position sensor head Position filter		
	Transmit commands to FGS	Pitch/Yaw Mode Acquire & Lock-on Select Stellar Magnitude	Lock-on Verify magnitude	Guide star acquired Fine Lock-on Verification Fine error	
	Transmit previous output Transmit commands to FGS	Deflection Calibration	Calibrate Image Dissector Calibration		Deflection Error Deflection Constant
	Transmit previous output Transmit commands to FGS	Deflection Reset	Reset Image Dissector Deflection Constant	Fine Lock-on Verification Fine Error	Deflection Constant
	Transmit previous output Transmit commands to FGS	Guide Star Coordinates Acquire and Lock-On	Lock-on at adjacent grating intersection for micrometer scale calibration	Fine Lock-on Verification Fine Error	
	Transmit previous output Identify star center for coarse scan, recompute star coordinates, transmit commands to FGS	Guide Star Coordinates Astrometry Mode (1) Exposure time	Perform coarse scan		- Photon Count Profile
	Transmit previous data Perform convolution Identify star centers for fine scan, recompute star coordinates Transmit commands to FGS	Guide Star Coordinates Astrometry Mode (2) Exposure time	Perform fine scan		Photon Count Profile
	Transmit previous data				
Data Analysis, using micrometer scale calibration data, fine scan photon count profiles, grating calibration data					

4.9 Data Storage And Processing Requirements

On-board data storage and processing requirements for astrometry with the fine guidance sensor depends upon which modes are used in the measurements. The storage and processing requirements in Table 4.9-1 are based upon measurement of stars ranging from M_V 17 to M_V 10 in brightness.

The fine guidance sensor used for astrometry primarily measures the positions of single stars. For measurements with the lock-on mode, the data storage requirements are minimal, since only the micrometer deflections plus status data need be recorded. The micrometer positions of the other two fine guidance sensors at the time of the measurement is included as part of the data. To measure the positions of up to 10 stars requires up to 100 (8 bit) bytes of storage. No on-board processing is required.

To measure the positions of up to ten stars using the fine scanning mode requires a maximum storage space of 3200 (8 bit) bytes with a maximum recording rate of 80,000 bits/second corresponding to M_V = 10. No on-board processing is required.

A routine is used to identify double stars by a preliminary course scan and on-board processing, so that star position data for both stars can be taken immediately, before the sensor head is moved to the next star position. This required additional storage of 10,000 (8 bit) bytes within the computer itself and 26,000 (multiply/add) operations within 10 seconds. Floating point capability is required.

This assumes that the on-board filtering is done using a stored kernel function, h(X,X'), which varies with the optical micrometer angle to account for the varying amount of aberration, rather than the Gaussian approximation to the function.

The computing power required for on-board processing of star positions is estimated in terms of the number of multiplications (*) and additions (+) required to perform a given algorithm along with the number of 32 bit memory locations required for working storage and program storage.

Approximately 200 locations would be required to store the raw data. If 10 signals are used to approximate the spatially varying kernel function h(X,X') and a linear interpolation scheme is used, a maximum of 2*10*20 = 400 locations would be required to store the interpolation constants exclusive of program storage for the interpolation program. If the interpolation program storage and the data acquisition program occupied an equal number of locations, an approximate fixed overhead of 100 locations is identified. The matched filter operation will require a maximum of 20*200 multiply/adds for the convolution along with an additional 8000 multiply/adds. Adding overhead for looping and summing will give approximately 10,000 */+ operations. An additional 200 output locations to collect the result is required. The maximum is selected and its position (d) determined by quadratic interpolation with about 1000 */+ estimated operations. After subtracting Max * h(X,d) from the result, the residual is examined for a second star peak by comparison to a threshold: estimated 1000 multiply/adds. If a second

TABLE 4.9-1

DATA STORAGE AND PROCESSING REQUIREMENTS WITHIN SSM FOR ASTROMETRY WITH THE FINE GUIDANCE SENSOR

MODE	DATA STORAGE* (8 Bit Bytes)	DATA PROCESSING*
Lock-On	100	None
Fine Scan	3200 (1600)	None
Coarse Scan and Star Identification (Optimum)	10000 (5000)	26000 (16000) mult/add operations
Coarse Scan and Star Identification (Single stored kernel functions)	3400 (1700)	26000 (16000) mult/add operations

* The larger numbers are based upon the scan times of Table 4.3-1 and photoelectrons counted from a M_V 10 star.

The numbers in parentheses are based upon the RMS center uncertainty of Table 4.3-1, with the scan time adjusted to the star magnitude. In either case, the performance of Table 4.3-1 would be met with a M_V 17 star.

star is encountered, the above is reiterated for an additional 1000 */+ to measure a binary star image. Net storage so far is 1200 locations and net execution time is 13000 (*/+). Using a factor of two for program size and execution, overhead yields 2400 locations and 26000 (*/+) operations. (To be more exact would require detailed algorithm and computer specifications.) A slow computer should be capable of 100 μsec per */+ yielding an execution time of 2.6 seconds. This is well within the fast scan time. The storage estimate is 10,000 bytes (8 bits) which is reasonable.

This computer requirement estimate is intended to represent the worst case (highest impact). Astrometry could be done with various levels of sophistication, ranging from no use of optical micrometer scanning to the method described above. Reducing the range of star magnitudes to be accommodated would reduce the amount of data to be processed. The above estimates are based upon a brightest star of M_V 10, giving a maximum count rate of 80,000 photoelectrons/second. For a single stored non-varying kernel function without interpolation, there would be 200 locations required to store the raw data, 20 locations for the single kernel function, and another 200 locations to store the result. This corresponds to 420 locations which when doubled and multiplied by $\frac{32 \text{ bits}}{8 \text{ bits/byte}}$ gives the required storage of 3400 bytes. The multiply/add requirements will be the same.

Further simplifications would involve the use of a single filter function with no interpolation as a function of micrometer angle, and the use of a simple square-wave filter function which would permit the convolution to be accomplished by addition alone. The latter simplification would increase the noise error by about a factor of 3 for a given scan time, or conversely, would require 10 times the scan time for a given noise error.

5.0 ASTROMETRY WITH THE ST

Table 5.0-1 summarizes the manner in which the principal astrometric tasks can be accomplished with various instruments on the ST. The main tasks are parallax and proper motion measurements, double star detection, and double star measurement. The instruments used are the fine guidance sensor, the area photometer or the faint object camera, the point photometer, and the focal plane camera. The primary mode of accomplishing each task is boxed in.

The fine guidance sensor is used primarily for parallax and proper motion measurements. As a matter of course, the coarse scan and fine scan modes will be used in the parallax and proper motion measurements because of the high probability of a second star biasing the measurement and because of the high probability of the stars being binary. Close double stars can be measured using spectral filtering and the fine scan technique. It is not expected that the fine guidance sensor will have the double star resolving capability of the area photometer or faint object camera.

The area photometer or the faint object camera would be the preferred instrument for resolution of close double stars whose existence is previously known. Spectral filtering is employed to take advantage of color separation of the stars in compensating the brightness difference. The point photometer is used in the special case of double star measurement by lunar occultation.

The focal plane camera is the instrument best suited to serendipitous detection of double stars. It is not expected that the fine guidance sensor will have a dynamic range significantly greater than that of the field camera, and the fine guidance sensor can investigate only predetermined stars, one at a time.

TABLE 5.0-1

ASTROMETRY WITH THE ST

	PARALLAXS AND PROPER MOTIONS	DOUBLE STAR DETECTION	DOUBLE STAR MEASUREMENT
Fine Guidance Sensor	Lock-On Coarse and Fine Scan (High Density Areas)	Coarse Scan	Fine Scan Spectral Filtering
Area Photometer or Faint Object Camera			F/96 Imagery Spectral Filtering
Point Photometer			Lunar Occultation
Focal Plane Camera		Serendipitous	

6.0 DESIGN VERIFICATION PLAN

The design verification plan for astrometry differs from that for the other scientific instruments because astrometry is accomplished with several non-dedicated instruments. The only astrometry hardware is the filter wheel, if it is included in the fine guidance sensor. In addition, the grating of the fine guidance sensor must be calibrated.

The test plan calls for qual testing of the filter wheel assembly, calibration of the fine guidance grating, testing the astrometric performance of the fine guidance sensor, the area photometer, and the field camera. Table 6.0-1 summarizes the plan, which is really just a modification to the test plans of the above-named instruments.

TABLE 6.0-1

DESIGN VERIFICATION PLAN

SUB ASSEMBLY LEVEL	BREADBOARD/ENG. MODEL	FLIGHT MODEL
Grating	Calibration	Calibration
Filter Assy	Qual Level Tests (SE)	Performance Tests
System	Performance Test (A)	Performance Test (A) Pre-Accept. Test (SE)

SE = Simulated Environment

A = Ambient

7.0 SUPPORT EQUIPMENT REQUIREMENTS

Special calibration hardware and software is required to calibrate the groove positions on the gratings of the fine guidance sensors. Aside from this, only the means to present double star images to the various instruments, and the software to command them in performing astrometric measurements and to reduce the data resulting are required. The double star simulation requirement is essentially an additional requirement on the test equipment required for the instruments used for astrometry. Table 7.0-1 summarizes the support equipment requirements.

TABLE 7.0-1

SUPPORT EQUIPMENT REQUIREMENTS

INSTRUMENT	SUB-ASSEMBLY LEVEL	REQUIREMENTS
Fine Guidance Sensor	Grating	Calibration Hardware and Software
	System	Double Star Simulation Means Command and Data Reduction Software
Area Photometer	System	Double Star Simulation Means Command and Data Reduction Software
Focal Plane Camera	System	Double Star Simulation Means Command and Data Reduction Software

GLOSSARY OF ACRONYMS

FGS - FINE GUIDANCE SENSOR

OTA - OPTICAL TELESCOPE ASSEMBLY

SI - SCIENTIFIC INSTRUMENT

SSM - SYSTEM SUPPORT MODULE

ST - SPACE TELESCOPE